Luigi CAVALERI(*) and Gerrit BURGERS(**)

Wind gustiness and wave growth

(*) Istituto Studio Dinamica Grandi Masse, S.Polo 1364, Venice, Italy

(**) K.N.M.I., De Bilt, The Netherlands

Abstract

We have analysed the consequences of wind gustiness on the growth of wind waves. Two mechanisms have been identified that enhance the usual Miles generation. The first one arises from the non negativity of the Miles mechanism and it is present only during the mature stage of a storm. The second is associated to the non linear dependance of the friction velocity on the wind speed and it is active throughout a storm cycle. The consequences of wind gustiness are found to be a faster growth and higher fully developed conditions, the increase being up to 30% in wave height. These findings are applied to a severe Mistral storm in the Mediterranean Sea and to a very strong event in the Northern Pacific ocean. Their application to wave modelling is discussed.

1 - Introduction

The growth of wind waves under steady wind conditions has been a subject of research for several decades. Starting from the theoretical approach by Miles (1957) and on the base of the results of several experiments (e.g. Hasselmann et al., 1973; Snyder et al., 1981) the problem is now relatively well understood. A number of formulas exist that provide a reasonable representation of the experimental wave growth rate. Given the input wind fields, these formulas are then applied to wave models to obtain a description of the space and time evolution of the wave field in a given area.

An implicit assumption in all the above steps is that the wind variability in space and time is slow enough to consider the wind as constant during each time integration step. However, while this is generally true at the synoptic scale, there is ample experimental evidence that this is not the case when we consider the short term local variability. Wind record at fix positions show oscillations of wind speed and direction around mean values that can be as high as 30% and 20 degree respectively (Monahan and Armendariz, 1971; Sethuraman, 1979). Fig.1 shows a wind record taken from an oceanographic tower in the Northern Adriatic Sea. The amplitude of the oscillations is evident.

The period of these oscillations can vary from a few seconds to several hours. The purpose of this paper is to study how the waves growth curve changes if one uses a wind that is not constant, but it fluctuates around average modulus and direction. To avoid any interference with the generation process itself, we

consider only fluctuations whose period is large respect to that of the dominant waves (we will see that the experimental evidence justifies this position). In practical terms we study a fluctuating generation.

It is worthwhile to point out that along the paper we use terms as turbulence, gustiness, wind variability, fluctuations. In the literature there is some distinction among them, usually based on frequency and depending on the subject under study. On the contrary, and with the aim to avoid excessive repeatitions, in this paper we make no distinction among them.

The paper is built as follows. In section 2 we give a short description of the physics involved by the process and we report a theoretical solution to the problem. The characteristics of a turbulent wind are analysed in greater details in section 3, and they are used for a further refinement of the theoretical approach. The same characteristics are then used to develop (section 4) a numerical solution of the problem. These findings are then applied to two real cases, hindcasting, with and without turbulence, a Mistral storm in the Mediterranean Sea and a very severe event in the Nortehrn Pacific ocean. The theoretical and numerical results are discussed in the final section 6, where we point out the conditions for their applicability.

2 - Theoretical background and solution -

In a classical paper Miles (1957) proposed a theoretical expression for the relation between the wind input and the wave variance spectrum. Snyder et al. (1981) fitted Miles theoretical curve to their experimental results, and they proposed a simple formula to approximate this curve. The WAM wave model (The WAM-DI Group, 1988) uses this formula for the wind input term, except that WAM follows Janssen and Komen (1985) in eliminating the wind speed at a fixed height in favor of the friction velocity. The wind input source term is then given by

$$S_{in} = 0.25 \frac{\rho_a}{\rho_w} \left[28 \frac{u_*}{c} \cos\theta - 1 \right] F(\omega)\omega \quad \text{if } \left(28 \frac{u_*}{c} \cos\theta - 1\right) > 0$$

$$= 0 \qquad \text{otherwise} \qquad (1)$$

Here F() is the wave variance spectrum, ω the angular frequency, θ the angle between the wave and wind directions, u_* is the friction velocity, and c is the phase velocity of waves with frequency ω. ρ_a/ρ_w is the air to water density.

In (1) the overall dependance on wind speed and direction is expressed in the bracketed term

$$\gamma = \left[28 \frac{u_*}{c} \cos\theta - 1 \right] \qquad (2)$$

The term ($28\ u_*$) is basically a different expression of the wind speed u at a given reference height. Hence the value of γ merely reflects the existing geometry between the phase speed of a wave and the wind speed component along its direction. So the

condition in (1) that $S_{in} = 0$ when $\gamma \leq 0$ simply reflects the physical fact that, to trasfer energy from wind to waves, the wind must blow faster than the wave phase speed. The opposite is not true because the Miles process dominates only in the "wind to waves" direction. As we will see later, this is a fundamental argument for the effect of wind turbulence on wave growth.

Equation (1) is certainly not the final answer to the question of the shape of the wind input term. In fact, alternatives have been proposed (e.g. Janssen, 1986; Kahma and Calkoen, 1991), but for all the frequencies except the very high ones they agree to within the experimental accuracy. Therefore we assume that if, instead of the WAM expression (1), we had used one of the alternatives, we would have obtained results very similar to the present ones. Therefore they can be considered to hold in general.

Consider now a wind field, fluctuating around some average value $\bar{u}_*$,

$$u_* = \bar{u}_* + \delta u_*$$

We want to derive the influence of the fluctuations on the growth curve of the waves.

There is a simple qualitative argument that the growth rate will be larger in this case than for a constant wind. Consider in fig.2 the plot of the γ factor (2) as a function of $\alpha = u_* \cos\vartheta / c$. For a given frequency, hence c, at the varying of u_*, hence α, the γ representative point moves along the oblique line. The threshold value of α, above which

the wind pumps energy into waves, is $\alpha_o = 0.0357$. For frequencies well above the threshold and small variations of u_*, and due to the linearity of (2), the effect of somewhat larger and smaller values of the friction velocity will almost cancel. But, for frequencies just above the threshold, the effect of a larger u_* and a larger γ is not canceled by the effect of a smaller u_* and a smaller γ because, according to (2), γ cannot be negative. Moreover, a frequency below the threshold value, which would get no wind input at all in the constant wind case, may now receive some wind input from time to time when the instantaneous wind is strong enough.

The above argument was analysed theoretically by Janssen (1986), who provided an expression for the effective wind input term for the case when the fluctuations of u_* can be described by a gaussian function. Following the theoretical analysis by Janssen (1986) we consider single time intervals over which the wave variance F() in (1) can be assumed to be constant. During such intervals the average wind input source term is given by

$$\bar{S}_{in} = \bar{\gamma}\ \omega\ F(\omega, \theta) \qquad (3)$$

with

$$\bar{\gamma} = \int_{-\infty}^{\infty} \gamma(u_*)\, p(u_*)\, du_*$$

$p(u_*)$ represents the probability distribution of u_*. Note that, because of the threshold limit discussed above and the non negativity of γ, we can have

$$\bar{\gamma} \geq \gamma(\bar{u}_*)$$

Defining $\sigma_{u_*}^2$ as the variance of the friction velocity, for gaussian fluctuations described by

$$p(u_*) = \frac{1}{\sigma_{u_*}\sqrt{2\pi}} \exp\left[-\frac{(u_* - \bar{u}_*)^2}{2\sigma_{u_*}^2}\right] \qquad (4)$$

we find the following expression for $\bar{\gamma}$,

$$\bar{\gamma}(u_*, \sigma_{u_*}) = \frac{1}{2}\left[1 - \mathrm{erf}(z)\right]\gamma_0(\bar{u}_*) + \frac{x(\sigma_{u_*}/\bar{u}_*)}{\sqrt{2\pi}} \exp(-z^2) \qquad (5)$$

with

$$z = \frac{1 - \bar{u}_*/c}{\sqrt{2}\, x(\sigma_{u_*}/\bar{u}_*)} \qquad x = 28\,\frac{u_*}{c}\cos\theta \qquad \mathrm{erf}(z) = \frac{2}{\sqrt{\pi}}\int_0^z e^{-t^2} dt$$

and $\gamma_0(u_*)$ given by (2).

Fig.3 shows the diagram of $\bar{\gamma}$ for different values of the percentual variability $\sigma_{u_*}/\bar{u}_*$. Note that, from now on and for the sake of simplicity, the $\cos\theta$ is neglected in the discussion. However the arguments strictly apply to $u \cdot \cos\theta / c$.

We see that the strongest effect is indeed around the threshold wind speed and frequency. The u_* fluctuations are mainly important for the growth of wave components in this area. In the early stages of development of a sea storm most of the energy is concentrated on frequencies located to the far right of the horizontal scale in fig.2. Consequently there will be no or little effect from the friction velocity fluctuations. As the waves evolve, and the peak moves to lower frequencies, the

energetic components approach the threshold value in fig.2, and they begin to feel the consequences of the unsteadiness of the wind. It follows that its effect is larger for an old that for a young wind sea.

The theoretical approach by Janssen (1986) is based on the implicit assumption that during each time interval, short enough to consider F() as constant, the variability of u_* can be described by a gaussian distribution. This possibility is strictly connected to the correlation existing between sequential wind values, and, for practical application in wave modelling, to the time step of the integration procedure (typically around 20 minutes). Before proceeding further we need therefore to explore more deeply the characteristics of a fluctuating wind field. This is done in the next section 3.

3 - Characterization of a wind field and modified theoretical approach

To characterize a turbulent wind field we refer to the available experimental data. There is ample evidence (see e.g. Munn, 1966, p.69) that the fluctuations of wind speed and direction around an average value are well represented by gaussian distributions. In our case this was checked by making a gaussian fit to a number of series of wind speed and direction values, obtained during a field experiment (the 1986 HEXMAX experiment off the Dutch coast, Smith et al., 1990). The correspondance proved to be excellent, as exemplified by fig.4,

in which a comparison is made between the experimentally found distribution of both wind speed and direction and gaussian distributions with the same mean value and standard deviation from an arbitrary HEXMAX record.

However this is not enough to fully characterize the wind field. Fig.5 compares a wind record (5a), actually the one used for the statistics in fig.4, with a random sequence (5c) with the same mean and distribution. There are evident differences, the main one being the pronounced oscillations present in the record, with a faster variability superimposed to them. The explanation lies in the correlation existing between sequential values of a wind record (see e.g. Munn, 1966, p.75). The physics of the process implies that wind values (speed and direction) at short time distance are not independent, but they must reflect only gradual changes. The shorter the time distance, the stronger the correlation. Similar arguments hold for space variability. If we want to have a realistic turbulent wind as input to a wave model, we have to model this correlation. This can be done as follows.

Given a sequence of random numbers a_i with zero mean, with a gaussian distribution and standard deviation σ_a, we can construct a derived sequence sequence b_i defined as

$$b_i = \alpha\, b_{i-1} + a_i \qquad (6)$$

with $0 \leq \alpha < 1$. It is shown (Box and Jenkins,1970,par.3.2.4, p.56) that b_i has zero mean and its variance is

$$\sigma_b^2 = \frac{\sigma_a^2}{1 - \alpha^2} \qquad (7)$$

Fig.5b shows a b_i sequence with the same statistical characteristics of sequences 5a and 5c. Its much stronger similarity with 5a is evident. The physical correspondance is stressed by the comparison in Fig.6 of the spectra from sequences 5a and 5b, and another record obtained from an oceanographic tower in the Northern Adriatic Sea (Cavaleri, 1979). The dashed line in Fig.6a approximates the mean spectrum obtained from a large number of b_i sequences. Note that the spectrum of the random a_i sequence would be a flat "white spectrum".

The proper value of α depends on the time step Δt of the sequence (Δt = 10 second implies a much higher α respect to, say, Δt = 5 minute) and on the characteristics of the wind we want to mimic. Large values of α lead to rather surprising results, as illustrated in fig.7, where the randomness of the process can, for large α values, be obscured by the extended time scale of the process, appearing as definite, even if temporary, trends of the field. As it will be pointed out in the final discussion, this has relevant consequences for practical applications. Fig.8 shows some wind sequences having the same correlation but different turbulence level.

We consider now the implications of the above characterization for the theoretical approach described in the previous section. It had been there assumed that the fluctuations δu_* around an average value $\bar{u}_*$ can be represented by a gaussian distribution. This had allowed the treatment in terms of erf function. However the available evidence is for a gaussian distribution of u rather than u_* (we are not aware of any experimental statistics for u_*). Still unable to express a

definite opinion on this point, we analuze the implications of a gaussian distribution of u.

The wind speed u (usually referred at the 10 metre height) and u_* are related via some drag law that for WAM (WAM-DI Group, 1988) has been taken as

$$u_* = c_d^{1/2} \cdot u$$

$$c_d = \begin{cases} (0.8+0.065\ u_{10}) \cdot 10^{-3} & \text{if } u_{10} > 7.5 \text{ m/s} \\ 1.2875 \cdot 10^{-3} & \text{otherwise} \end{cases} \qquad (8)$$

Other authors have proposed different expressions for c_d (see e.g. Amorocho and DeVries, 1980 and Smith, 1988), but in all the cases c_d is a growing function of u_{10}.

If u and u_* are related by a non linear law as (8), a gaussian distribution of u excludes a similar one for u_*. The consequent difference in distribution is examplified in fig.9 by the distribution of u implied by an eventual gaussian distribution of u_*. We see that a given $\sigma_* = \sigma_{u_*} / \bar{u}_*$ for friction velocity corresponds to a lower $\sigma = \sigma_u / \bar{u}$ value for the wind speed. Besides, the associated u distribution is asimmetrical, with a negative skewness.

Given the distribution of u, using (8) we can deduce numerically the one of u_*, $p'(u_*)$. We can then recover the theoretical approach, provided that in (3), instead of the gaussian distribution (4), we use $p'(u_*)$. This leads to a numerical evaluation of $\bar{\gamma}$ as a function of u_* and $p'(u_*)$, i.e. of u and its turbulence level.

Given the fact that c_d is a growing function of u, it follows that u_* grows faster than u. From (8), for large u values, $u_* \sim u^{3/2}$. This reveals a second mechanism by which the turbulence can increase the wave growth rate. Every simmetric oscillation of u is reflected into a non simmetric oscillation of u_*, skewed towards the high values. From (2) this leads to an average $\bar{\gamma}$ larger than the one corresponding to the undisturbed (non turbulent) friction velocity. Therefore the turbulence can enhance the wave growth rate not only in the well developed stage for the intermittancy of the generation process, but also in the early stage of growth, as well as throughout the storm, for the non linearity of u_*, and consequently of the γ factor in (2), respect to u. A positive Δu leads to a relative gain of energy larger than what is lost for a correspondingly negative Δu.

The modified distribution of γ is shown in fig.10 a,b, and it can be compared with the one in fig.3. Around the threshold value the behaviour is similar, the curves in fig.10 b being actually slightly higher than in fig.3, as expected. Note that a direct detailed comparison is not possible because, unlike fig.3, in fig.10 the curves depend on the wave frequency considered. However the major differences are present on the high frequency part of the diagrams (large u_*/c or u/c values). While in fig.3,

i.e. under the hypothesis of a gaussian distribution of u_* , the curves collapse to the non turbulent case, in fig.10, with a gaussian distribution of u, the curves remain differentiated; besides they tend to increase their differences while moving towards the higher u/c values.

4 - Numerical approach -

For the numerical tests on the effect of wind variability on wave growth we have used a single point version of the third generation WAM wave model. The model is throughly described by the WAM-DI Group (1988), and we will limit here ourselves to a compact description of its basic principles.

The model is based on the numerical integration of the energy balance equation. The source function includes all the main mechanisms affecting the energy budjet of the field, i.e. generation by wind, non linear energy transfer among different wave components, and various dissipation processes. The basic idea of the model, within the limits of the present knowledge, is to avoid any parametrization and to describe each process on a pure physical basis. The model provides at each grid point the standard 2-d spectrum (25 frequencies and 12 directions are used) plus all the derived quantities (1-d spectrum, significant wave height H_s , mean period T_m , etc.).

The single point version neglects the advection and it limits itself to the integration of the source function. In so doing we virtually assume an infinite ocean with a wind uniform in space and variable in time. So we are actually considering a time limited generation. As wind input we have used sequences of numbers generated by (6). The average a, and b, value is 20, but different values of correlation α and standard deviation σ_b have been used. We have found a time step Δt = 60 second a convenient trade-off between resolution in time and computer time requirements. While different α values have been used for test purposes, comparison with experimental results has suggested the value α =0.9.

In showing the results of the numerical tests we will proceed in two steps. We will first present the cases with no correlation (α =0) and different level of percentual wind variability $\sigma = \sigma_u / \bar{u}$. We will then stick at a given variability, and we will show the consequences of using different α values. The 20 m/s mean wind speed used for all the tests corresponds by (8) to u_* =0.92 m/s.

Fig.11 shows the growth curve of H_s for different levels of wind variability. The effect is dramatic. A 10% variability increases H_s of only a few percents after three days, but σ =0.3 causes H_s to increase of about 30% (i.e. 70% in energy), with H_s still far from the saturation level.

As previously deduced from the qualitative and theoretical analysis the wind variability does not produce strong effects in the early stages of development. The curves begin to

differentiate substantially at about half development of the reference curve (σ =0), and when, after 72 hours, this is approaching the asymptotic value, the σ =0.2 and σ =0.3 curves are still actively growing. The slowness of the process in the last two cases is explained by the intermittancy of the wind input in the lower frequencies (figs.2 and 10 b).

The differences deriving from the assumption of a gaussian distribution of the wind or friction velocity are evident in fig.11, showing also the consequences of the gaussian variability of u_* for the case σ =0.3. As expected from the theoretical arguments discussed in the previous section, we see that a gaussian assumption on u_* produces a lower wave height.

The tests with a variable wind modulus have been repeated for direction. We have found that a 5 degree spread on the input field produces hardly any difference. However a 25 degree spread, very large respect to what effectively measured in the field, leads to a 10% decrease of the final H_S value. We have found also a particularly negative effect in the early stages of development. The principal reason for this comes from the γ expression (2). A variation in direction implies a variation of ϑ. Because of the non linearity of the cosine function, concave downwards in the section of interest, the integral of the energy input during an oscillation is smaller than in the constant case. As the $\cos\vartheta$ coefficient, $28 \cdot u_* / c$, is larger for high frequencies (small c values) and the directional spread wider, the effect is larger during the early stages of growth.

The spectra of the gusty growth curves are similar to the JONSWAP type of the ordinary wind sea, with a tendency to have some more energy on the low frequency side. This is what we expect from the physics of the process. This affects slightly the relationship between H_s and the peak frequency f_p. For the same f_p, a variable wind leads to somewhat higher wave heights respect to the constant wind case.

We move now to the second part of the numerical test, i.e. we stick at a fix value of wind variability, namely $\sigma = 0.25$, and we consider the consequences of a different correlation in time. Given the previous results, we consider only variability of the wind modulus, with a constant direction.

The results are shown in fig.12, and they can be better understood referring to the input winds shown in fig. 7. Note that, because the different curves oscillate around the same mean line, to be clearly distinguishable they have been shifted up of 2 metre each.

The correlation causes long oscillations of the significant wave height, superimposed to the general trend. It is remarkable that the mean trend hardly changes, as seen from the comparison with the $\alpha = 0$ case, associated to each curve as a smooth line. An increase of the value of α causes a strong increase of the H_s oscillations, whose amplitudes reaches 20% of the present H_s value in the $\alpha = 0.90$ case (much larger for larger α).

All the previous tests have been executed with a time step $\Delta t = 60$ second. We have done quite a bit of testing to verify the sensitivity of the growth curve to the Δt value and the correct relationship with α. Some of the tests with $\alpha = 0$ have been repeated with Δt values between 1 and 1200. Clearly the tests with very low Δt have no physical significance; they are simply useful to check the numerical procedure. The results have shown that the growth curve is not sensitive to the different Δt values. For $\alpha > 0$ and for the largest values (600, 1200 second) a certain expected randomness becomes apparent, with only slightly higher final H_s values for the smaller Δt.

About the $(\Delta t, \alpha)$ values we have already mentioned that comparison with measured data have suggested to correctness of the couple (60, 0.9). With the same Δt higher values of α have also been used for the tests shown in fig.12. Clearly to be consistant an increase of Δt implies a decrease of the α value and viceversa. Given the b_i sequence in (6), it is shown (Box and Jenkins, 1970, par.3.2.4, p.56) that the autocorrelation is α between sequential points, and α^k between points k steps apart. Given a reference couple $(\Delta t_o, \alpha_o)$, it follows that the $(\Delta t, \alpha)$ relationship for any Δt is

$$\alpha = \alpha_o^{(\Delta t / \Delta t_o)}$$

5 - Practical applications -

Mistral storm

We have applied our findings to a strong Mistral storm that took place in the Western Mediterranean Sea in December 1988. The Mistral is a violent cold northerly wind that enters the Mediterranean Sea through the Carcassone passage, between Spain and France. It is extremely active, and it produces some of the heaviest storms in this area (Cavaleri et al., 1991).

The event of December 1988 was the first burst of cold air of the season. Blowing on still relatively warm water, it led to highly unstable conditions, hence to strong turbulence. We are not aware of any detailed study of the atmospheric turbulence over the sea as a function of air-sea stability conditions. For its quantification we have followed Monahan and Armendariz (1971) and Sethuraman (1979). The formers found the gustiness to be a function of lapse rate, the higher gustiness being present for highly unstable conditions. For such conditions they found $\sigma = \sigma_u / \bar{u} = 0.2 - 0.3$. Similarly Sethuraman (1979), from the measurements done off Long Island, on the east coast of US, during hurricane Belle, reports σ values varying between 0.2 and 0.37 as a function of air-sea temperature difference. Further indications were obtained from the analogue wind records, similar to the one shown in fig.1, obtained from the oceanographic tower in the Northern Adriatic Sea and the corresponding air-sea temperature differences.

During the December 1988 storm different conditions were present along the fetch. On the northern part, off the coast of France (see fig.13), the water temperature t_a was estimated at 15 °C, while the air temperature t_w was 5 °C (from the Climatological Atlas of the Western Mediterranean, ENEA 1990, and

the meteorological maps of the Deutsche Wetterdienst respectively). In the most southern part of the fetch both air and water temperature were higher, with a slightly smaller absolute difference. This was in favour of a higher degree of turbulence in the northern part. On the other side the wind speed was decreasing while moving from the French to the African coast (see fig.13), and this counteracted the previous effect on the distribution of turbulence (σ decreases with increasing wind speed, see Monahan and Armendariz, 1971). We decided therefore to assume a constant $\sigma_u/\bar{u}$ ratio for the whole fetch, that, on the base of available data, was fixed at 0.25. We have kept this value constant also throughout the storm. This is likely to have introduced some approximation in the early and last stages of the hindcast period (2 days of warming up and tail were allowed at both ends of the storm), but we believe this did not affect the heart of the storm, and it was therefore irrelevant for the test.

The two hindcasts, without and with turbulence, are shown in fig.14 (actually peak conditions are shown). A comparison between the two reveals the similarity of the wave fields at short fetches, off the French coast, with growing differences while moving to the South. This is what we expected from the results shown in fig.11, as the same argument on the higher excitement of low frequencies holds for both time and fetch limited generation. The correspondance is well evidenced by the distribution of H_s along the fetch, shown in fig.15.

Wave height measurements were available at Diendjelli, on the Algerian coast, shown with a dot in fig.14 b. The measured H_s at the peak of the storm is reported in fig.15. On the whole, when compared to the Diendjelli data, the "turbulent" hindcast has an average error of -.24 metre, compared to -.89 metre of the "no turbulence" case.

The "turbulent" hindcast was done with the tecnique described in the previous paragraph, i.e. with a time step of 60 second and, at each single grid point, a 0.9 correlation between the sequential wind values. We have not allowed any variability in direction. Due to the arguments expressed in the previous section about the consequences of using different Δt, the differences seen in figs.14 and 15 are considered as due only to the introduction of turbulence.

Pacific storm

A second test on the effect of turbulence in a real storm was done, in a much larger scale, for a severe storm occurred in the Northern Pacific ocean in November 1988. A first storm was active around the Aleutinian Islands on November 2, producing a large area of swell moving towards South-South-East. Between 4 and 5 November the swell crossed another stormy area, North-West of Hawaii, producing very large waves. Both the storms were characterized by northerly wind blowing on relatively warm water, hence by very unstable conditions. The meteorological situation at 12 UTC 5 November 1988 is shown in fig.16. Isolines of wind speed are traced at 4 m/s interval. The maximum speed is above 28 m/s.

Our main aim during the test was to verify the sensitivity of the standard WAM model to the introduction of turbulence. Consequently the usual 3 degree resolution was used.

The results from the standard (no turbulence) hindcast, at the peak of the storm, are shown in fig.17a. The large waves area, West of Hawaii, is quite evident in the central low part of the figure. A number of wave recording buoys were active in the area at the time; the position of the one closest to the track of the storm is shown by a small circle in fig.17a. The comparison between the measured and model H_s data is in fig.18a. There is an evident underestimate of the significant wave height throughout the storm.

The hindcast was repeated with the introduction of 25% turbulence, using a time step of 5 minute. The results are shown in figg. 17b and 18b. There is a 2 metre increase of the significant wave height at peak conditions, and a much better fit between measured and model data. The bias and the r.m.s. error for H_s pass from -0.39 and 0.90 metre for the non turbulent case to the corresponding figures of 0.26 and 0.80 metre of the repeated hindcast (see Table I for a full intercomparison). However the improvement is better than this. The effect of turbulence should expectably be present only in the bunch of waves coming from the northern storm described above. The low wave situations preceeding and following the storm were not of northern origin, and consequently not generated in the highly unstable conditions that characterized the main event. For a proper check of the results it is therefore logical to compare the measured data with a combined hindcast, made by the non

turbulent results substituted by the turbulent ones for the period of the storm, i.e. on 4, 5 and 6 November. In so doing we find a drastic improvement (see Table I), the bias being reduced to -0.09 metre and the r.m.s. error to 0.70 metre. It is worthwhile to point out that most of the r.m.s. error derives from the peak H_S value recorded at 06 UTC of 5 November.

Finally it is of interest to analyse the evolution of the wave height along the track followed by the patch of energy across the two storms. The dots in fig.17b represent the position of the patch, at 12 hour interval, as deduced by the WAM hindcast. The wave height history is shown in fig.19. We see that the two fields were already well differentiated at 00 UTC of 3 November, close to the Aleutinian Islands (see fig.17b). The difference kept slightly decreasing with decreasing wave height while propagating South. On the 4th the waves system reached the area of the second storm, close to the Hawaiian Islands, and it began immediately to grow again. The difference too began to increase rapidly again, both because of the more intense generation in turbulent conditions, and of the wind acting on an already higher sea.

Daily applications

For daily application it is not acceptable to work with one or five minute time step: the model would become umbearably time consuming. We have to devise how to introduce the effect of wind variability when using a 20 minute (or similar value) time step. A possible solution is the modified theoretical approach described in sections 2 and 3. However this is not enough; the

wind spectra, as those shown in fig.6, indicate the presence of energy at periods larger than ΔT = 20 minute. This has to be accounted for on a numerical basis, with a suitable choice of the $\sigma_u/\bar{u}$ value and of the α correlation. Obviously now $\bar{u}$ represents the average over 20 minutes.

An indication of $\sigma_{\bar{u}}$, i.e. of the energy present at frequencies lower than f=1/ΔT, is obtained considering the wind spectrum. Sticking for convenience to an analytical expression, we consider the spectrum of the b_i sequence (6) given by Box and Jenkins (1970, par.3.2.4., p.56) as

$$S(f) = \frac{2\sigma_a^2}{1 + \alpha^2 - 2\alpha\cos(2\pi f \Delta t)}$$

The integral of S(f) (see Abramowitz and Stegun, 1970, 4.3.133) can be expressed as

$$\sigma_{\bar{u}}^2 = \sigma_u^2 \frac{2}{\pi} \operatorname{atan}\left(\frac{1+\alpha}{1-\alpha} \tan \pi f \Delta t\right)$$

where $\sigma_{\bar{u}}^2$ is the variance to the left of f. Taking f=1/ΔT=1/1200, and equalling angle with tangent because of its very small value, we find

$$\sigma_{\bar{u}}^2 = \frac{1}{600} \frac{1+\alpha}{1-\alpha} \sigma_u^2$$

Using as before α =0.9 we have

$$\sigma_{\bar{u}}^2 \simeq \frac{1}{50} \sigma_u^2$$

i.e.

$$\sigma_{\bar{u}} \simeq \frac{1}{7} \sigma_u$$

To apply expression (4) to sequential 20 minute averages $\bar{u}$ we still need to know the corresponding correlation value α. Given the correlation α between sequential single values, we have analysed the correlation between sequential groups of n elements. We have found (the calculations are given in the appendix) that $\bar{\alpha}$ has a value slightly higher than the one between single values at n steps distance. The corresponding diagrams are given in fig.20.

6 - Discussion -

The results given in sections 2, 3 , 4 and 5 show clearly the effect of wind variability on the growth rate of wind waves. The effect is limited in the early stages of growth, but it leads to a substantial increase of energy in the intermediate and final stages. A small percentual variability of wind speed, $\sigma_u/\bar{u} < 0.1$, has little effect; larger $\sigma_u/\bar{u}$ values, of order 0.3, lead up to a 70% increase of the overall waves energy. The variability in direction slows down the growth rate, particularly in the early stages of growth, but on the whole its effect is not as relevant as that due to the variability of the wind speed.

The quantification of the effects of wind turbulence, summarized in the diagrams of figs.11 and 12, relies on the assumption that expression (1), as derived from the Bight of Abaco experiment, refers to cases of no turbulence. If this were not the case the data should be scaled down accordingly to obtain

the zero reference from which to evaluate the effective input term. Snyder has pointed out (personal communication) that during the Bight of Abaco experiment the wind turbulence did not receive much attention. However it is conceivable that this did not affect the final results, i.e. expression (1), because the estimates of growth rate were obtained not from an analysis of the growth curve, but from measurements of wave coherent atmospheric pressure fluctuations. Therefore we assume (1) as valid for $\sigma = 0$ and figs.11 and 12 as effectively representative of the waves response to a fluctuating wind. It is clear anyhow that this point has to be carefully considered when analysing wind generation data to deduce practical formulas similar to (1).

We have considered the possibility that the growth curve due to a turbulent wind is adimentionally connected to the standard one. The WAM model we have used for the tests is suitable to explore this possibility, as its physics is scale invariant (WAM-DI Group, 1988). Sequences of the same dimensionless winds will give the same dimensionless spectra, provided that all the quantities are made dimensionless by multiplication with an appropriate combination of u_* (or u) and of the acceleration of gravity. One of the consequences of this scaling is that log-log plots of nondimensional growth curves have identical shapes. We wondered whether the gusty growth curve for an average friction velocity u_* with gustiness σ_{u_*} would be the same as the ordinary growth curve for a somewhat larger wind speed u'_* and no gustiness. This turned out not to be the case. In fig.21 we compare three growth curves. Two of them have no gustiness and

different values of u_*, one of them has a relative gustiness of $\sigma_{u_*}/\bar{u}_* = 0.3$. The shape of the gusty growth curve is markedly different from the one of the ordinary growth curves.

For the hindcast of the Mistral storm described in section 5 we have made a rough estimate of the turbulence level on the base of the expected air-sea temperature difference and the relative indications from the literature. However it is obvious that, if the turbulence is to be considered in wave modelling on a regular basis, the related information, concerning its level and frequency distribution, must be provided by the large scale meteorological models, certainly with a higher accuracy than it is done today.

The characteristics of the turbulence affect also the correlation in time of the wind, and consequently the evaluation of the effective increase in wave energy. There is an increasing demand of improved results from the meteorological models, particularly close to the surface. The dependance of the wind drag coefficient on the air-sea stability conditions is another typical example. We expect that the problem will find a solution with the coupling of meteorological and oceanic models.

One evident consequence of the wind variability on the growth curve of wind waves is that their growth is not smooth. The irregular oscillations superimposed to the average growth trend merely reflect the ones of the wind. Their amplitude depends on the variability of the wind σ_u and, as seen in fig.12, they can be as high as 20% of the actual H_s value. These oscillations are a common finding in the wave height

records during a very active storm. Due to their stochastic character there is no hope to reproduce them by a wave model, even introducing the turbulence in the input wind fields. This implies a minimum r.m.s. error that must be taken into account when judging the performance of a wave model.

Appendix

Correlation between blocks of sequential correlated values

We are given a sequence of numbers x, of unit variance for simplicity, such that

$$< x_j \cdot x_{j+k} > = \alpha^k \qquad (1)$$

The quantity α^k is the correlation between two numbers k points apart. In particular α is the correlation between sequential numbers.

We consider now the grouping of x into blocks of n elements and the average $\bar{x}$ value in each block. We seek the correlation $\bar{\alpha}$ between sequential $\bar{x}$ values (one block includes the 1 to n numbers, the other the n+1 to 2n ones).

$\bar{\alpha}$ is given by

$$\bar{\alpha} = < \frac{x_1 + \cdots + x_n}{n} \cdot \frac{x_{n+1} + \cdots + x_{2n}}{n} > \qquad (2)$$

Given (1), (2) is exploited as:

$$\bar{\alpha} = \frac{1}{n^2} \left(\alpha^n + \alpha^{n+1} + \cdots + \alpha^{2n-2} + \alpha^{2n-1} + \right.$$
$$\alpha^{n-1} + \alpha^n + \cdots + \alpha^{2n-3} + \alpha^{2n-2} +$$
$$\cdots\cdots\cdots\cdots$$
$$\alpha^2 + \alpha^3 + \cdots + \alpha^n + \alpha^{n+1} +$$
$$\left. \alpha + \alpha^2 + \cdots + \alpha^{n-1} + \alpha^n \right) =$$

$$= \frac{1}{n^2} \left(\alpha + 2\alpha^2 + 3\alpha^3 + \cdots + (n-1)\alpha^{n-1} + n\alpha^n + (n-1)\alpha^{n+1} + \right.$$
$$\left. + \cdots + 3\alpha^{2n-3} + 2\alpha^{2n-2} + \alpha^{2n-1} \right)$$

Using

$$\alpha \frac{d}{d\alpha}\left(\frac{1-\alpha^{n+1}}{1-\alpha}\right) = \sum_{0}^{n} k\alpha^k = \sum_{1}^{n} k\alpha^k$$

we obtain

$$\bar{\alpha} = \frac{1}{n^2}\left[\sum_{1}^{n} k\left(\alpha^k + \alpha^{2n-k}\right) - n\alpha^n\right]$$

Posing $\beta = 1/\alpha$

$$\bar{\alpha} = \frac{1}{n^2}\left[\alpha \frac{d}{d\alpha}\left(\frac{1-\alpha^{n+1}}{1-\alpha}\right) + \alpha^{2n}\beta \frac{d}{d\beta}\left(\frac{1-\beta^{n+1}}{1-\beta}\right) - n\alpha^n\right]$$

$$= \frac{1}{n^2}\left[-\frac{n\alpha^{n+1}}{1-\alpha} + \frac{\alpha-\alpha^{n+1}}{(1-\alpha)^2} - \alpha^{2n}\frac{n\beta^{n+1}}{1-\beta} + \alpha^{2n}\frac{\beta-\beta^{n+1}}{(1-\beta)^2} - n\alpha^n\right]$$

$$= \frac{1}{n^2}\left[-\frac{n\alpha^{n+1}}{1-\alpha} + \frac{\alpha-\alpha^{n+1}}{(1-\alpha)^2} + \frac{n\alpha^n}{1-\alpha} + \frac{\alpha^{2n+1}-\alpha^{n+1}}{(1-\alpha)^2} - n\alpha^n\right]$$

$$= \frac{\alpha}{n^2}\left(\frac{1-\alpha^n}{1-\alpha}\right)^2$$

Figure captions

1 - Analogue wind record from an oceanographic tower in the Northern Adriatic Sea. Speed in knot, direction in degree. The amplitude of the oscillations is evident.

2 - Plot of $\gamma = 28\, u_* \cos\theta/c - 1$ as a function of $u_* \cos\theta/c$. When close to the threshold value for which $\gamma = 0$, the oscillations of u_* make γ temporarily negative.

3 - Effective input term as a function of turbulence level $\sigma = 0.10,\ 0.20,\ 0.30$ respect to the no turbulence case $\sigma = 0.00$ according to Janssen (1986).

4 - a) wind speed distribution - diamonds: measured data; crosses: gaussian distribution. b) as a), but for direction.

5 - Sequences of wind speed. a) measured data from the HEXMAX experiment (used for statistics in fig. 4a). b) random numbers with the same statistical distribution as a), and .9 correlation between sequential numbers. c) as b), but with no correlation between sequential numbers.

6 - Spectra of wind data. a) measured in the Northern Adriatic Sea. b) measured during the HEXMAX experiment (see figs. 4a and 5a). c) synthetic (see fig. 5b).

7 - Sequences of synthetic wind data with the same turbulence level, but different correlation between sequential numbers.

8 - Sequences of synthetic wind data with the same correlation between sequential numbers, but different turbulence level.

9 - Distribution of wind speed u_{10} for an assumed gaussian distribution of the friction velocity. Two different cases are shown.

10 - a) Effective wind input term as a function of turbulence level σ =0.10, 0.20, 0.30 respect to the no turbulence case σ =0.00. b) as a), but focused on the threshold value. The diagrams depend on the frequency considered.

11 - Growth curves resulting from different levels of wind turbulence with a gaussian distribution of u. A very small integration step has been used to smooth the curves. The dotted line, for the case σ =0.30, shows the consequences of a gaussian distribution of u_* .

12 - Growth curves resulting from a 0.25 wind turbulence level. Different correlation α between sequential wind values has been used, the smooth reference lines corresponding to α =0.00. There is a 2 metre up shift of each diagram for better visualization.

13 - Mediterranean Sea. Wind field at 00 UT of 16 December 1988.

14 - a) Wave field at the same time of fig.13. Wind turbulence has not been considered. b) as a), but with a 0.25 wind turbulence level. The dash line shows the section along which H_S is plotted in fig.15. The dot identifies the location of Diendjelli, where measurements were available.

15 - Distributions of H_S along the fetch marked in fig.14b. Non turbulent (a) and turbulent (b) case. The small circle shows the value measured at Diendjelli (see fig.14b).

16 - Northern Pacific ocean. Wind field at 12 UTC 5 November 1988. Isolines of wind speed are shown at 4 m/s interval.

17 - Wave field at the same time of fig.16. a)non turbulent wind, b)turbulent wind. The dots show the previous positions of the waves system at 12 hour interval.

18 - Comparison between measured wave height (open squares) and model results (dots); a)non turbulent wind, b)turbulent wind. The measuring position is indicated with a small circle in fig.17a.

19 - Evolution of the height of the waves system present West of Hawaii Islands on 5 November 1988. Its positions at 12 hour interval are shown by dots in fig.17b. Non turbulent (a) and turbulent (b) case.

20 - Correlation between single data k points apart or sequential groups of k points each. A 0.9 correlation between sequential numbers has been assumed.

21 - Nondimensional growth curve for: (continuous lines) u_* =0.48 and 0.8 m/s, corresponding respectively to u=12 and 18 m/s; no turbulence; (dotted line) u_* =0.8 m/s; σ =0.30.

Table I

Statistics of goodness of results for the turbulent, non turbulent and mixed hindcast of the Hawaiian storm of November 1988.

	bias (m)	rms error (m)
non turbulent	-0.39	0.90
turbulent	0.26	0.80
combined	-0.09	0.80

References

Abramowitz,M. and I.A.Stegun, 1970, "Handbook of mathematical formulas", Dover Publications, Inc.,New York, 1046 pp.

Amorocho, J., and J.J.De Vries, 1980,"A new evaluation of the wind stress coefficient over water surfaces", J.Geoph.Res., Vol.85, no.C1, pp.433-442.

Box, . and Jenkins, 1970, "Time series analysis, forecasting and control", Holden Day, S.Francisco, 553 pp.

Kahma,K. and Calkoen,C., 1991, "Reconciling discrepancies in the observed growth of wind-generated waves", submitted to J.Physic.Ocean.

Cavaleri,L, 1979, "An instrumental system for detailed wind wave study", Il Nuovo Cimento, Serie 1, Vol. 2C, pp.288-304.

Cavaleri,L., L.Bertotti and P.Lionello, 1991, "Wind wave-cast in the Mediterranean Sea", J.Geoph.Res., Vol.96, C6, pp.10739-10764.

ENEA, 1990, "Climatological Atlas of the Western Mediterranean Sea", Internal Report, Rome, 224 pp.

Hasselmann,K., T.P.Barnett, E.Bows, H.Carlson, D.E.Cartwright, K.Enke, J.A.Ewing, H.Gienapp, D.E.Hasselmann, P.Kruseman, A.Meersburg, P.Muller, D.J.Olbers, K.Richter. W.Sell and H.Walden, 1973, "Measurements of wind-waves growth and swell decay during the Joint North Sea Wave Project (JONSWAP)'', Dtsch. Hydrog. Z., A 8 (12), 95 pp.

Janssen,P.A.E.M., 1986, "On the effect of gustiness on wave

growth", Report 00-86-18 Kon.Ned.Met.Inst., De Bilt, The Netherlands, 17 pp.

Janssen,P.A.E.M. and G.J.Komen, 1985, "Effect of atmospheric stability on the growth of surface waves", Bound. Layer Meteor., vol.32, pp.85-96.

Janssen,P.A.E.M., P.Lionello, M.Reistad and A.Hollingsworth, 1989, "Hindcasts and data assimilation studies with the WAM model during the Seasat period", J. Geoph. Res., vol.94, no.C1, pp.973-993.

Miles, J.W., 1957, "On the generation of surface waves by shear-flows", J. Fluid Mech.,3, 186, pp.185-204.

Monahan and Armendariz, 1971, "Gust factor variations with height and atmospheric stability", J.Geoph.Res., Vol.76, no.24, pp. 5807-5818.

Munn, R.E., 1966, "Descriptive micrometeorology", Academic Press, N.Y., 245 pp.

Sethuraman,S., 1979, "Atmospheric turbulence and Storm surge due to Hurricane Belle (1976)", Monthly Weather Review, vol.107, no.3, pp.314-321.

Smith, S., 1988, "Coefficients for sea surface wind stress, heat flux and wind profiles as a function of wind speed and temperature", J.Geoph.Res., vol.93, no.C12, pp. 15467-15472.

Smith,S.D., K.B.Katzaros, W.A.Oost and P.G.Mestager, 1990, "Two major experiemnts in the humidity exchange over the sea (HEXOS) program", Bull. of the Am.Met.Soc., 71, pp.161-172.

Snyder,R.L., F.W.Dobson, J.A.Elliott and R.B.Long, 1981, "Array measurements of atmospheric pressure fluctuations above surface gravity waves", J. Fluid Mech., pp.102, 1-59.

The WAM-DI Group, 1988, "The WAM model - a third generation ocean prediction model", J. Phys. Ocean., vol.18, no.12, pp.1775-1810.

Acknowledgments

The ideas developed in the paper have matured through long discussions with our collegues and friends Peter Janssen and Piero Lionello.

The two single point versions of the WAM model used for the tests have been provided by K.N.M.I. and Piero Lionello.

R.Kraan and W.Oost have provided the data of the HEXMAX experiment.

Luciana Bertotti has helped with part of the graphics.

The hindcast of the Mistral storm has been executed at the European Centre of Medium Range Weather Forecasts, in Reading, U.K. The wind fields have been kindly provided by the U.K. Meteorological Office.

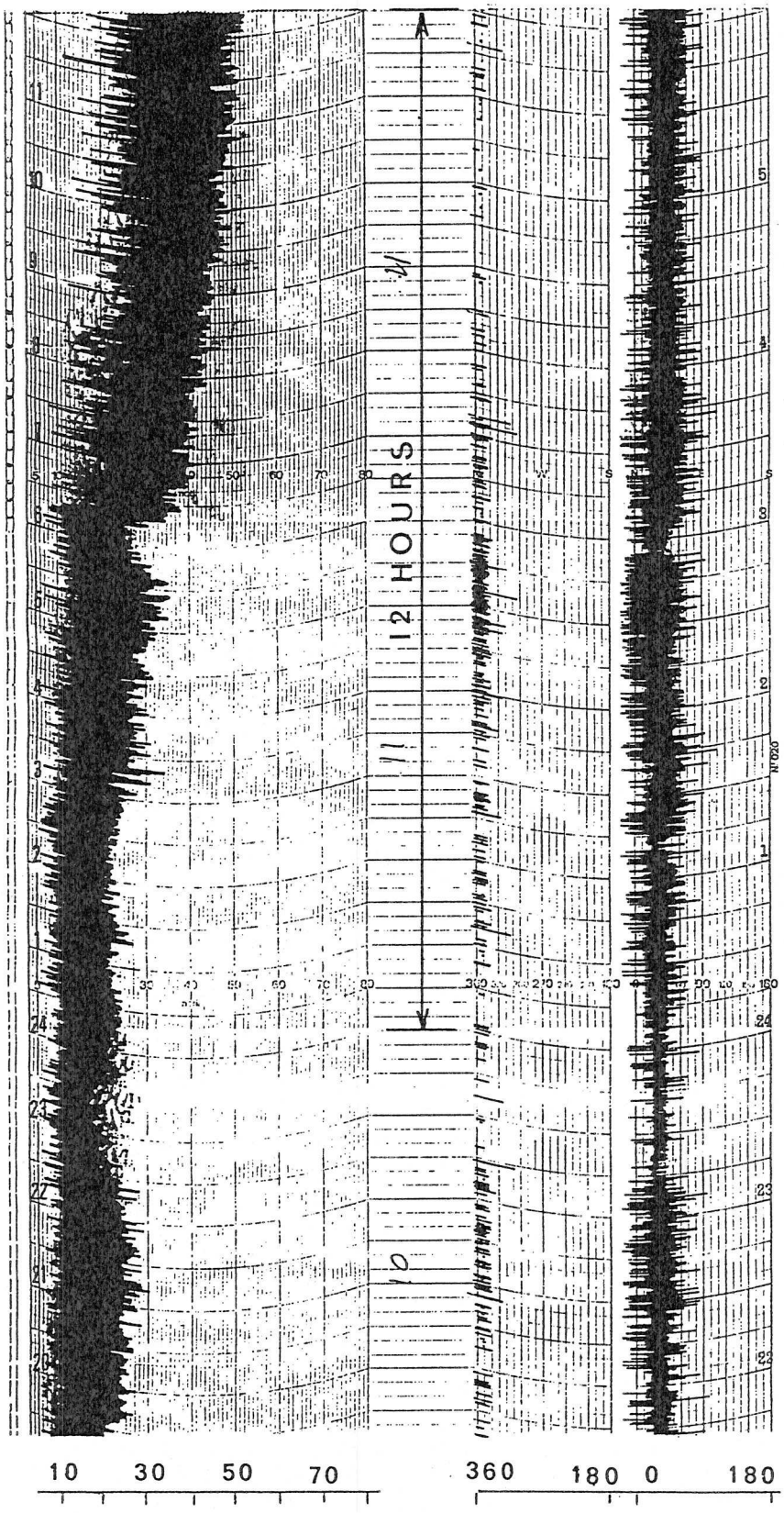
12 HOURS
10 30 50 70
360 180 0 180

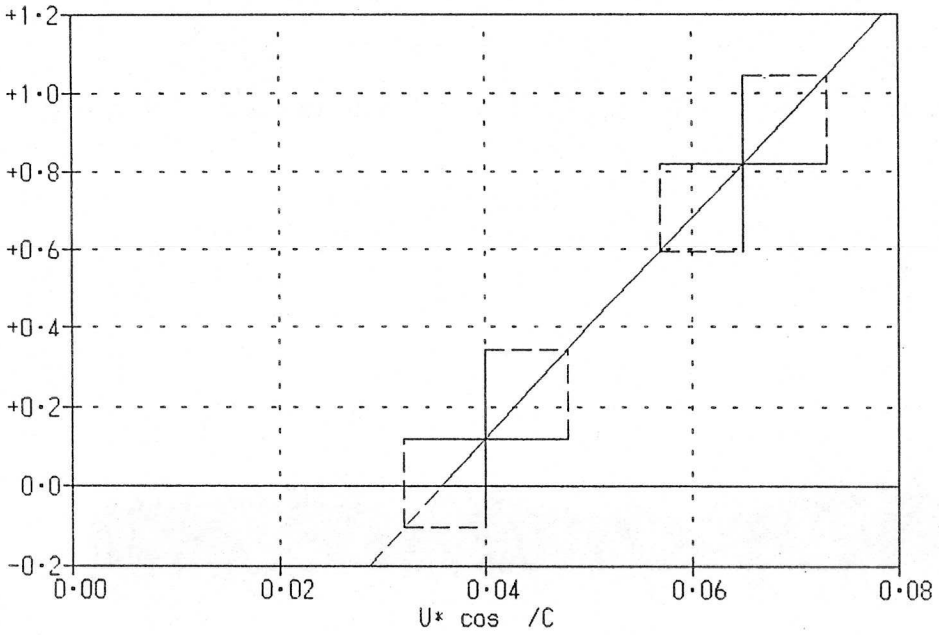
+1·2
+1·0
+0·8
+0·6
+0·4
+0·2
0·0
-0·2
0·00
0·02
0·04
0·06
0·08
U* cos /C

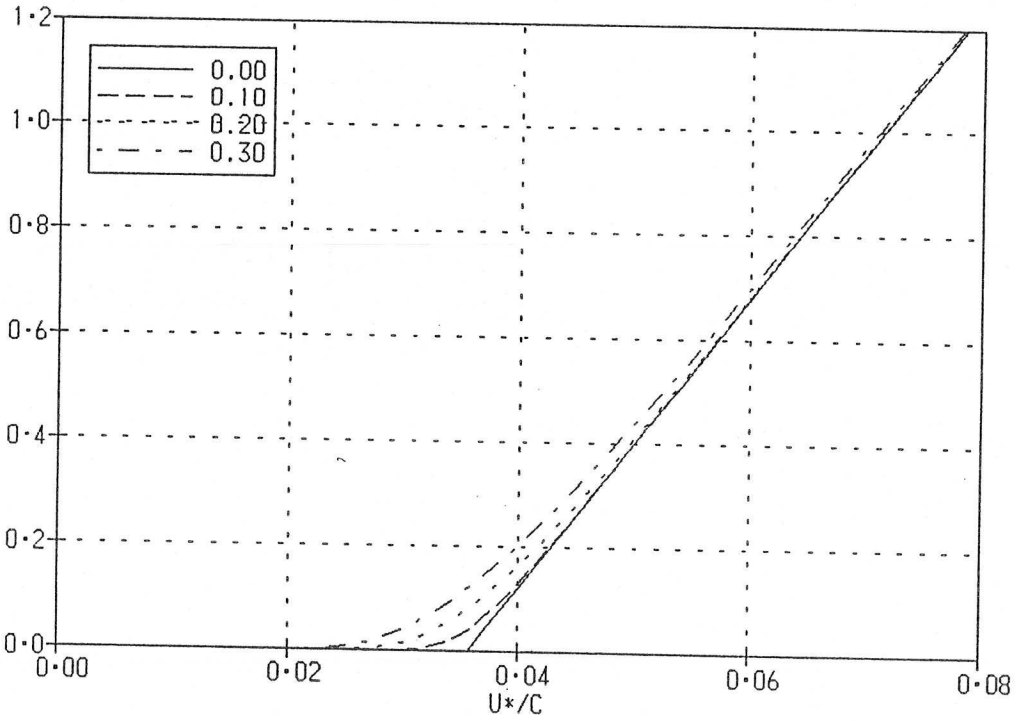
0.00
0.10
0.20
0.30
1·2
1·0
0·8
0·6
0·4
0·2
0·0
0·00
0·02
0·04
0·06
0·08
U*/C

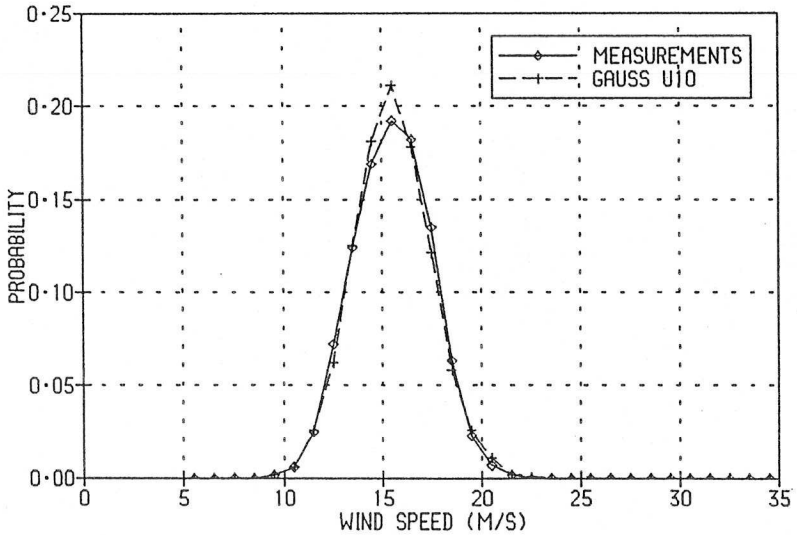
0·25
0·20
0·15
0·10
0·05
0·00
PROBABILITY
0
5
10
15
20
25
30
35
WIND SPEED (M/S)
MEASUREMENTS
GAUSS U10

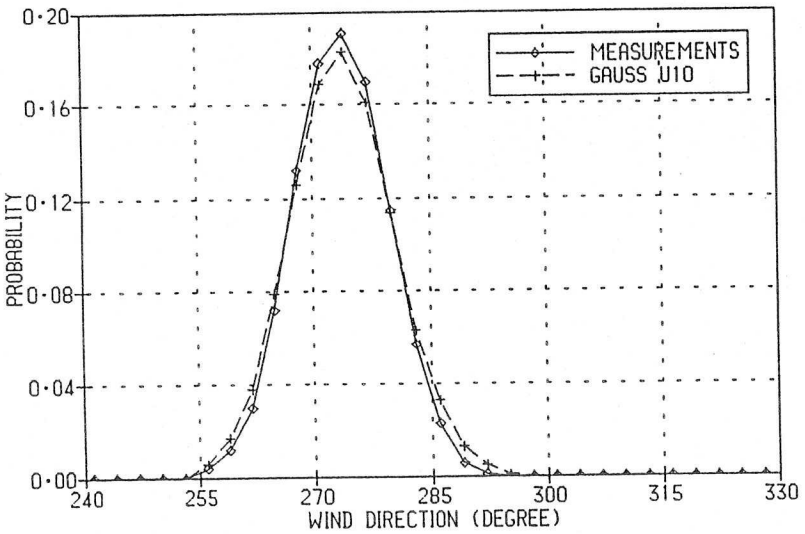
MEASUREMENTS
GAUSS U10
PROBABILITY
0·20
0·16
0·12
0·08
0·04
0·00
240
255
270
285
300
315
330
WIND DIRECTION (DEGREE)

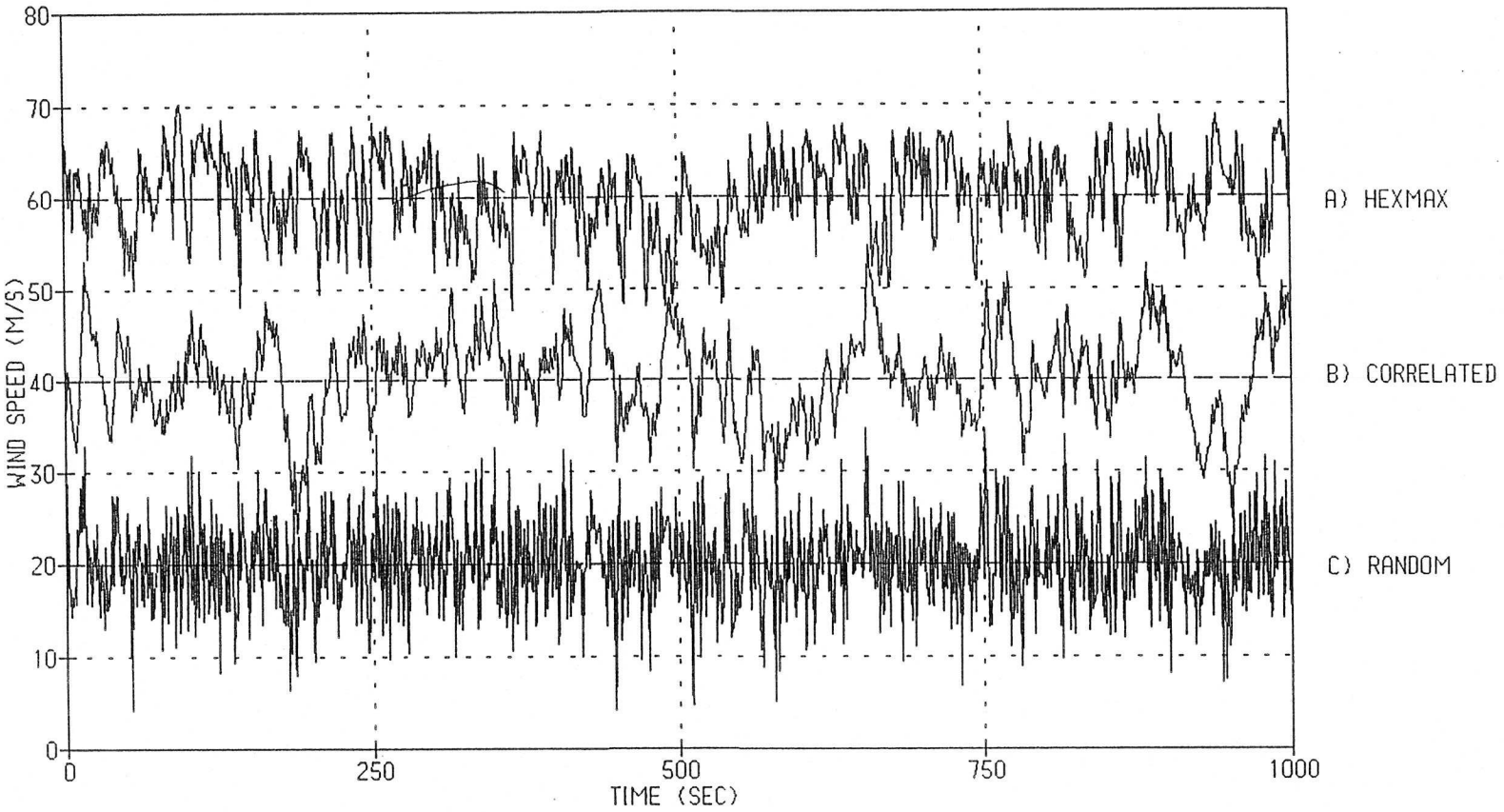
80
70
60
50
40
30
20
10
0
WIND SPEED (M/S)
0
250
500
750
1000
TIME (SEC)
A) HEXMAX
B) CORRELATED
C) RANDOM

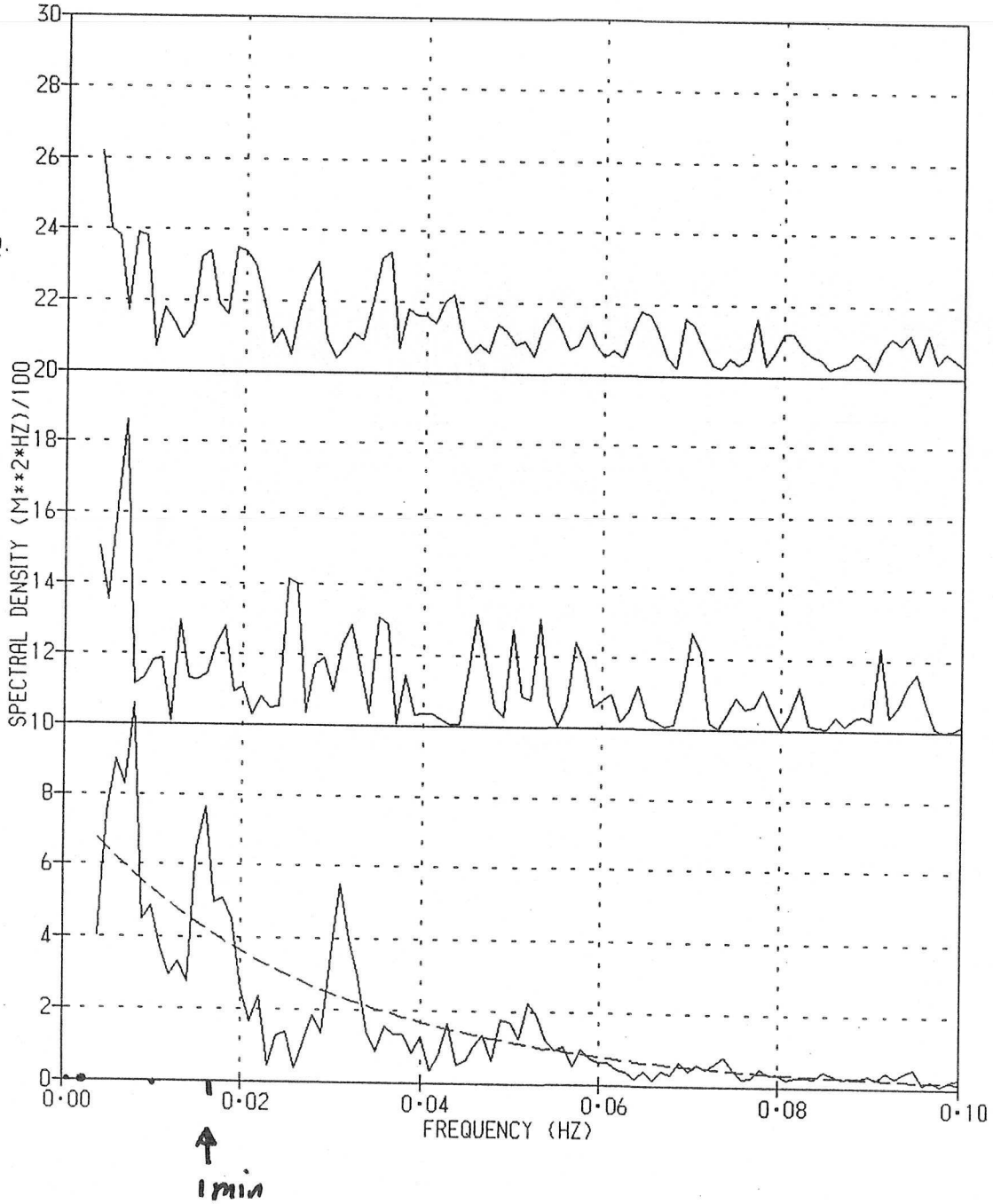
30
28
26
24
22
20
18
16
14
12
10
8
6
4
2
0
SPECTRAL DENSITY (M**2*HZ)/100
0·00
0·02
0·04
0·06
0·08
0·10
FREQUENCY (HZ)
C) ISDGM TOWER
B) HEXMAX
A) CORRELATED
1 min

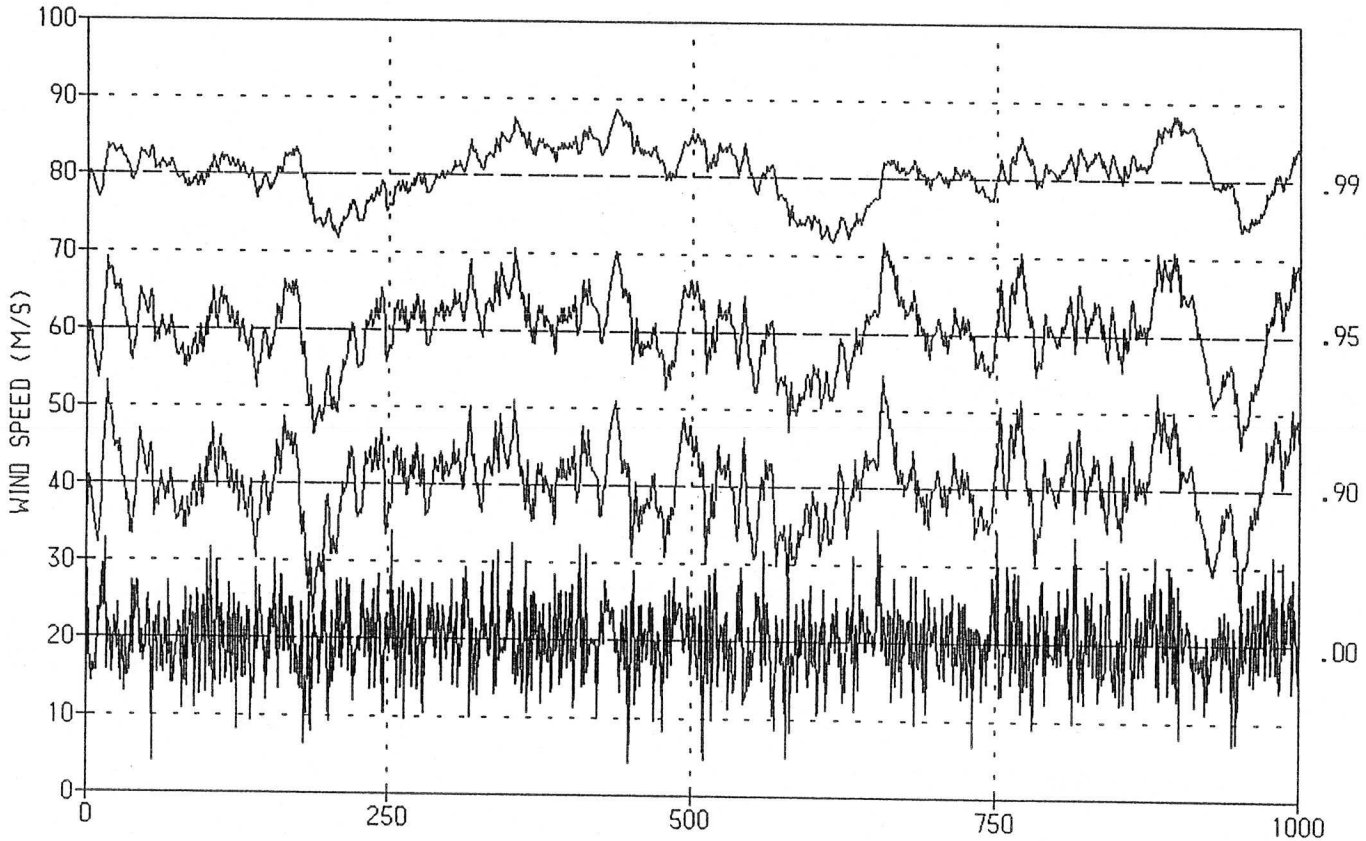
100
90
80
70
60
50
40
30
20
10
0
WIND SPEED (M/S)
0
250
500
750
1000
.99
.95
.90
.00

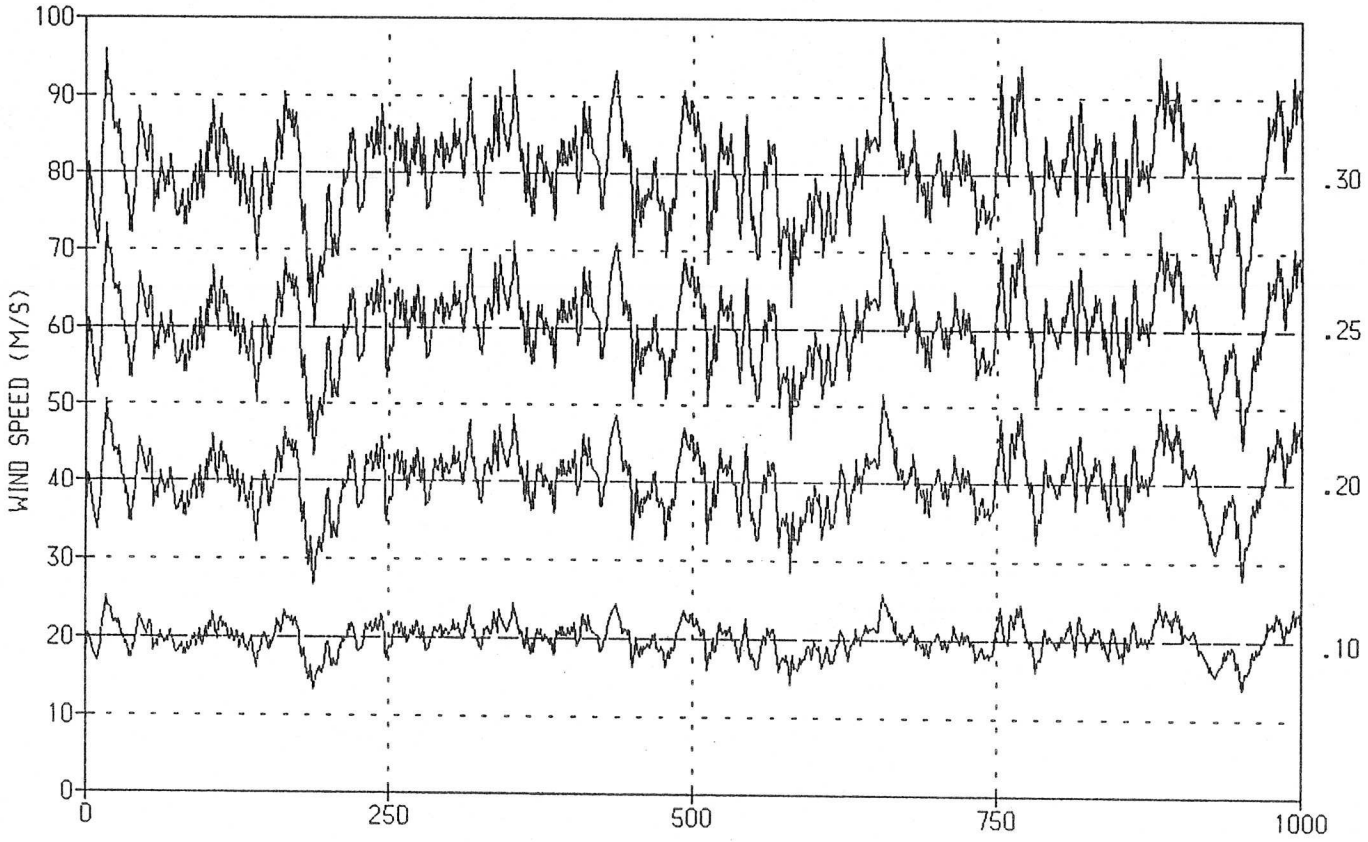
WIND SPEED (M/S)
100
90
80
70
60
50
40
30
20
10
0
0
250
500
750
1000
.30
.25
.20
.10

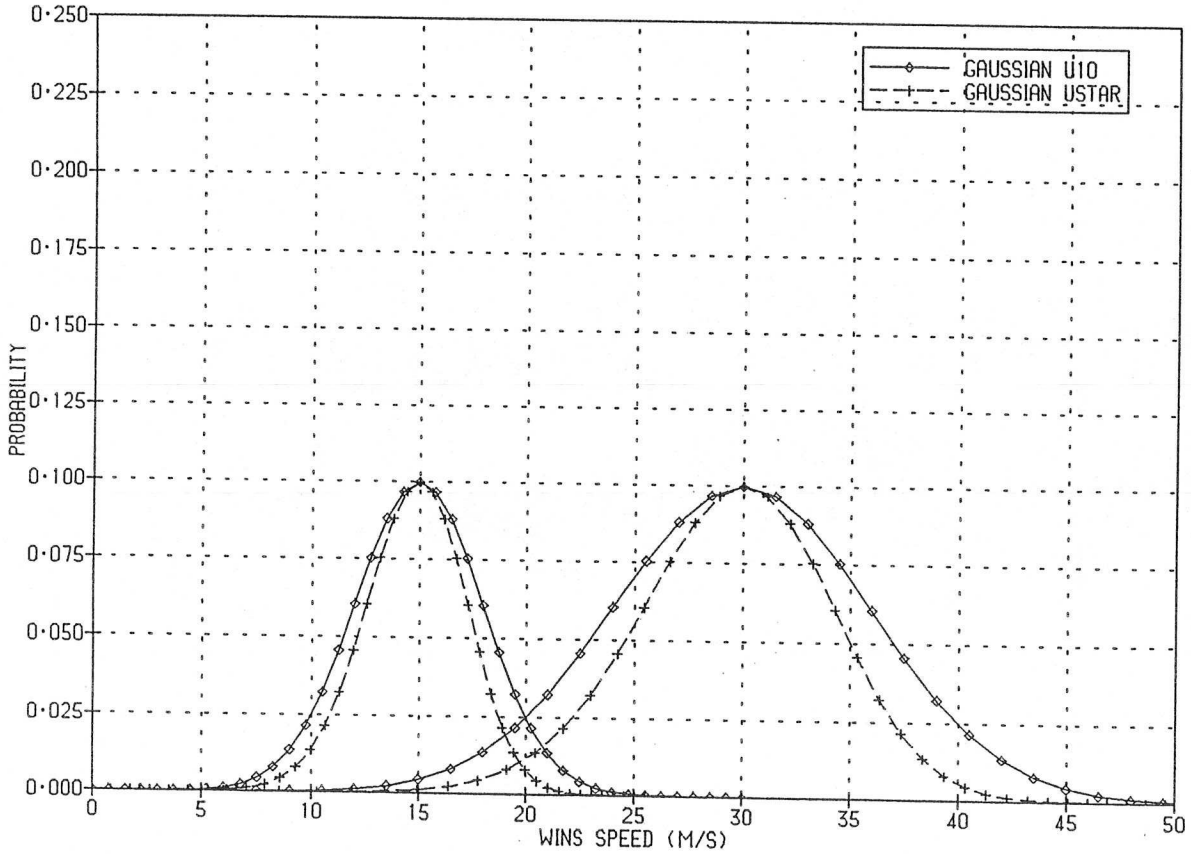
GAUSSIAN U10
GAUSSIAN USTAR
PROBABILITY
0·250
0·225
0·200
0·175
0·150
0·125
0·100
0·075
0·050
0·025
0·000
0
5
10
15
20
25
30
35
40
45
50
WINS SPEED (M/S)

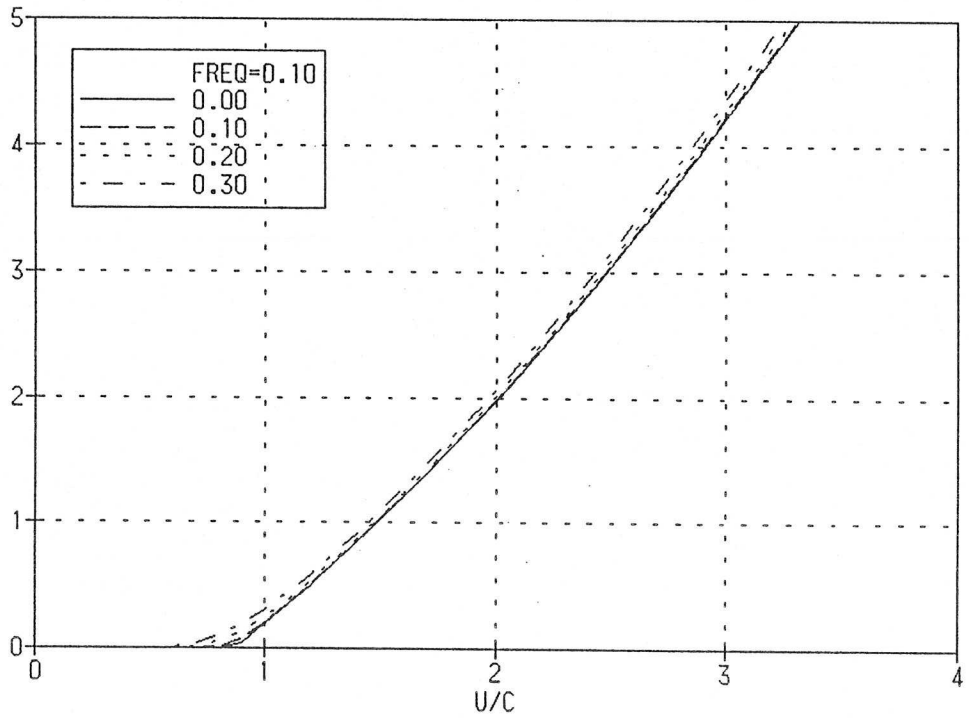
FREQ=0.10
0.00
0.10
0.20
0.30
5
4
3
2
1
0
0
1
2
3
4
U/C

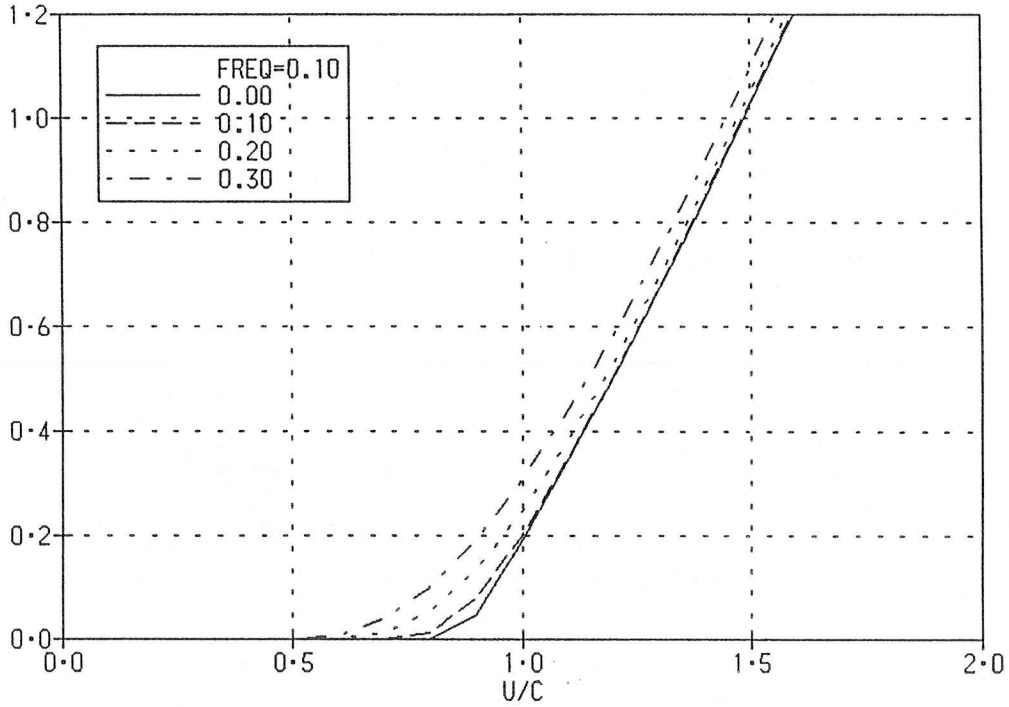
FREQ=0.10
0.00
0.10
0.20
0.30
1·2
1·0
0·8
0·6
0·4
0·2
0·0
0·0
0·5
1·0
1·5
2·0
U/C

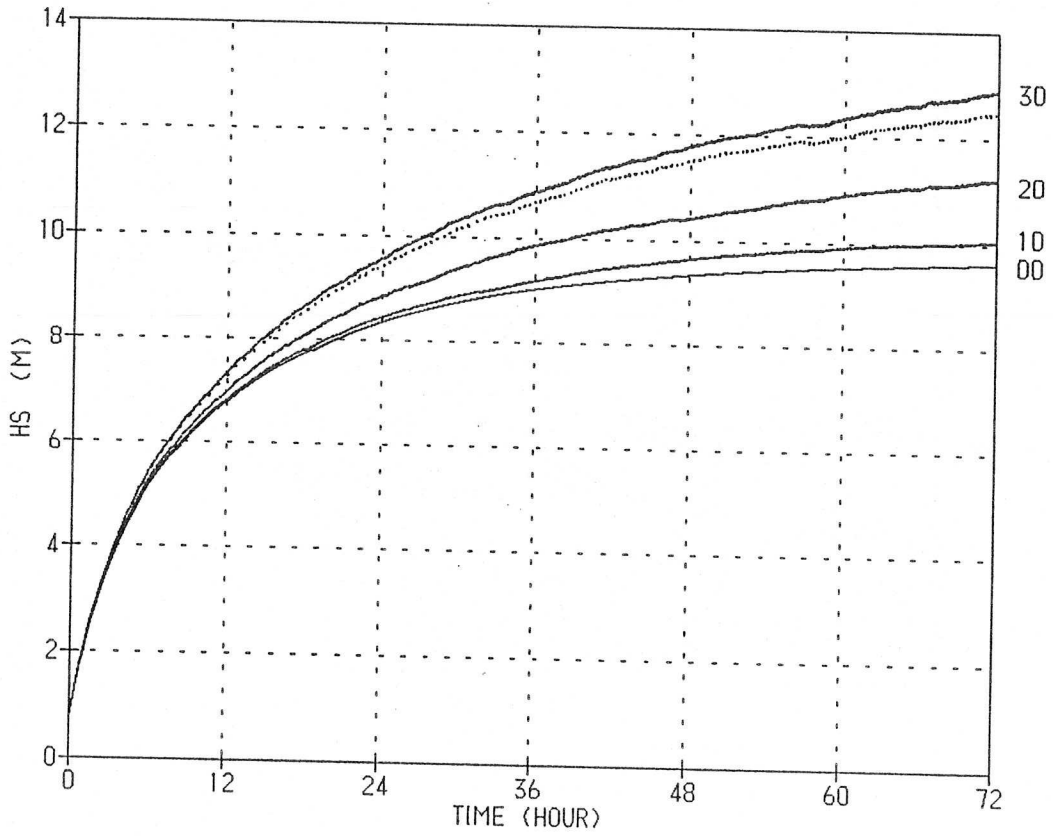
14
12
10
8
6
4
2
0
HS (M)
0
12
24
36
48
60
72
TIME (HOUR)
30
20
10
00

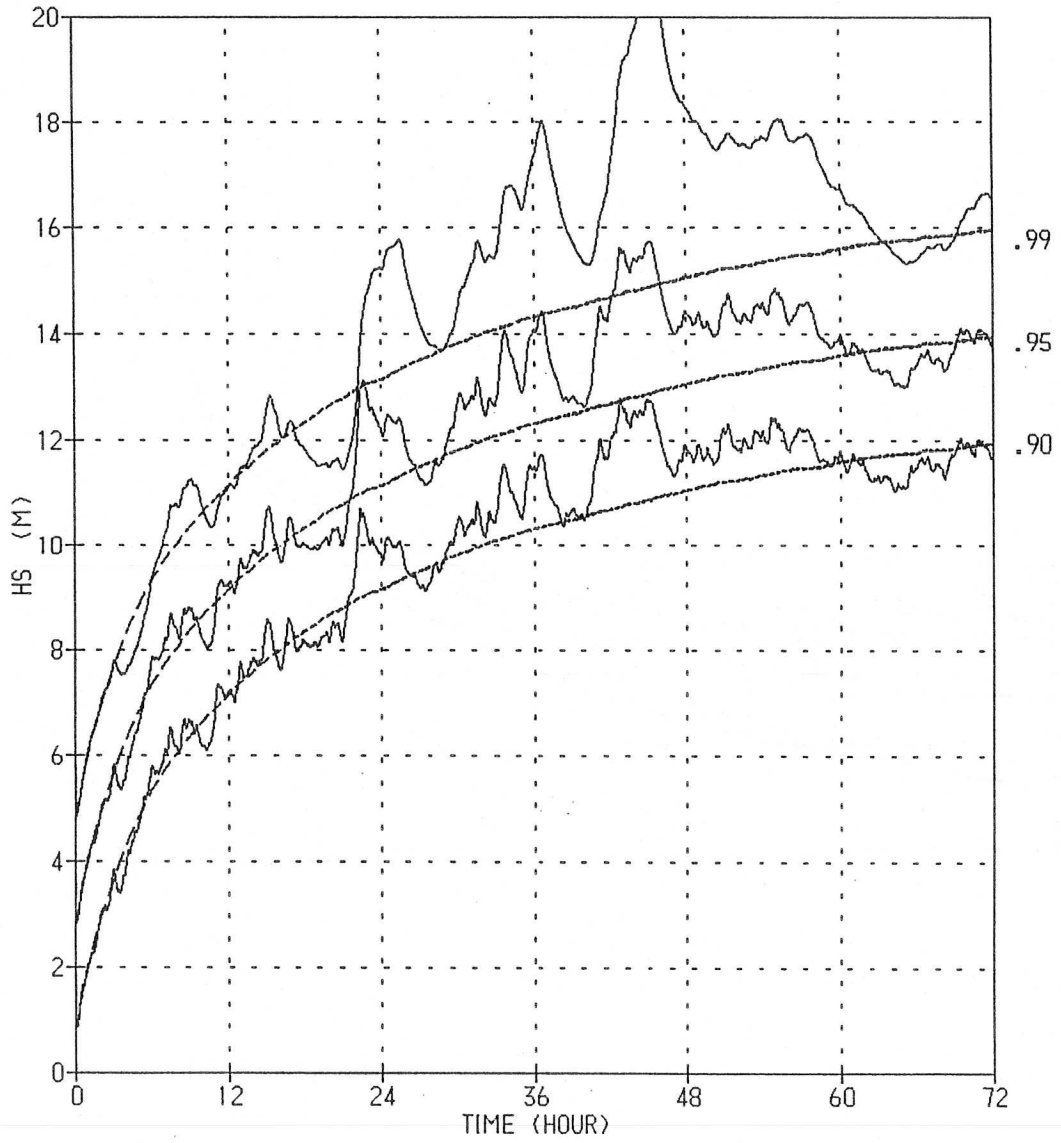
20
18
16
14
12
10
8
6
4
2
0
HS (M)
0
12
24
36
48
60
72
TIME (HOUR)
.99
.95
.90

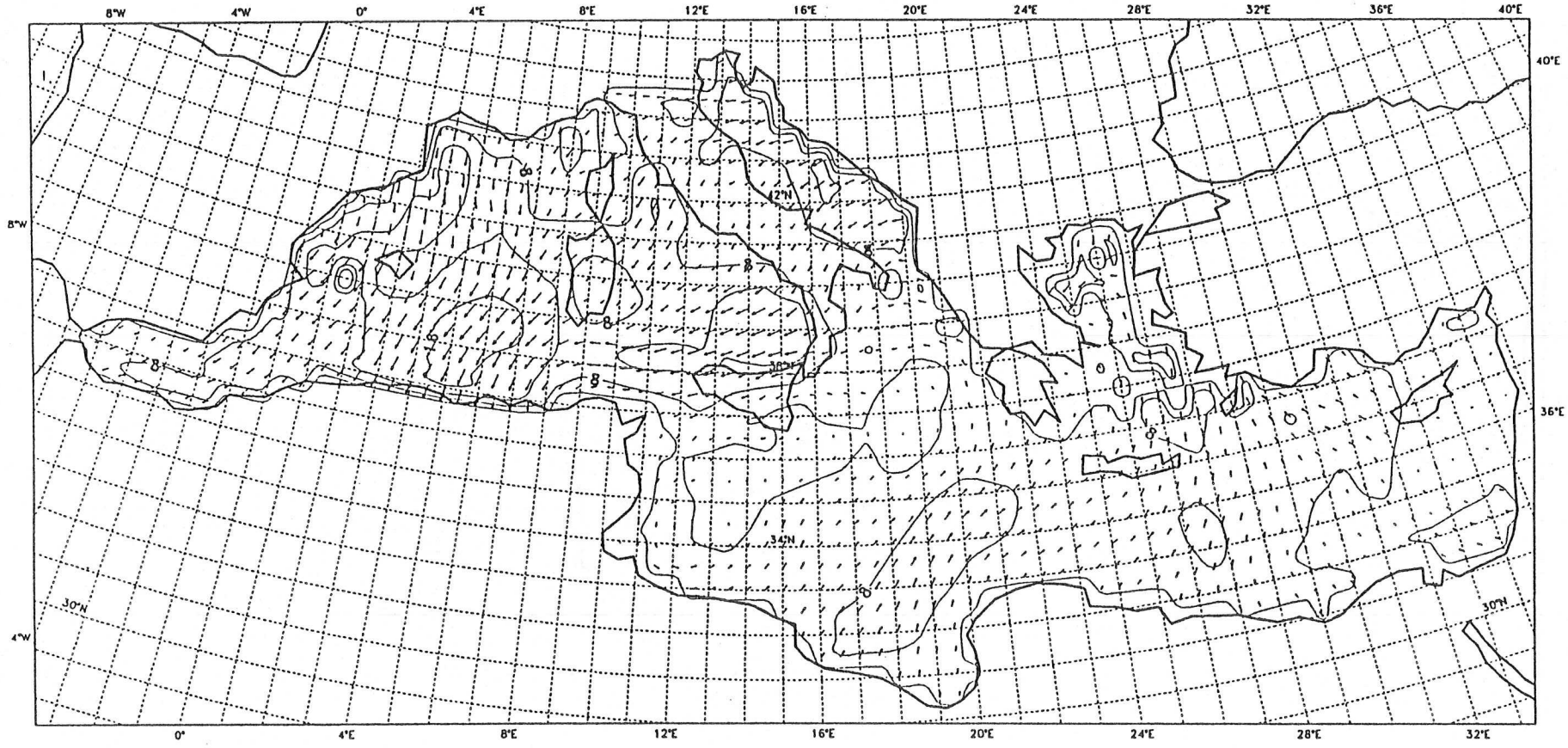
MEDITERRANEAN SEA – 10M WIND AT 1988.12.21 06 UT
8°W
4°W
0°
4°E
8°E
12°E
16°E
20°E
24°E
28°E
32°E
36°E
40°E
42°N
38°N
34°N
30°N

MEDITERRANEAN SEA – WAMS WAVE HEIGHT AT 1988.12.21 06 UT

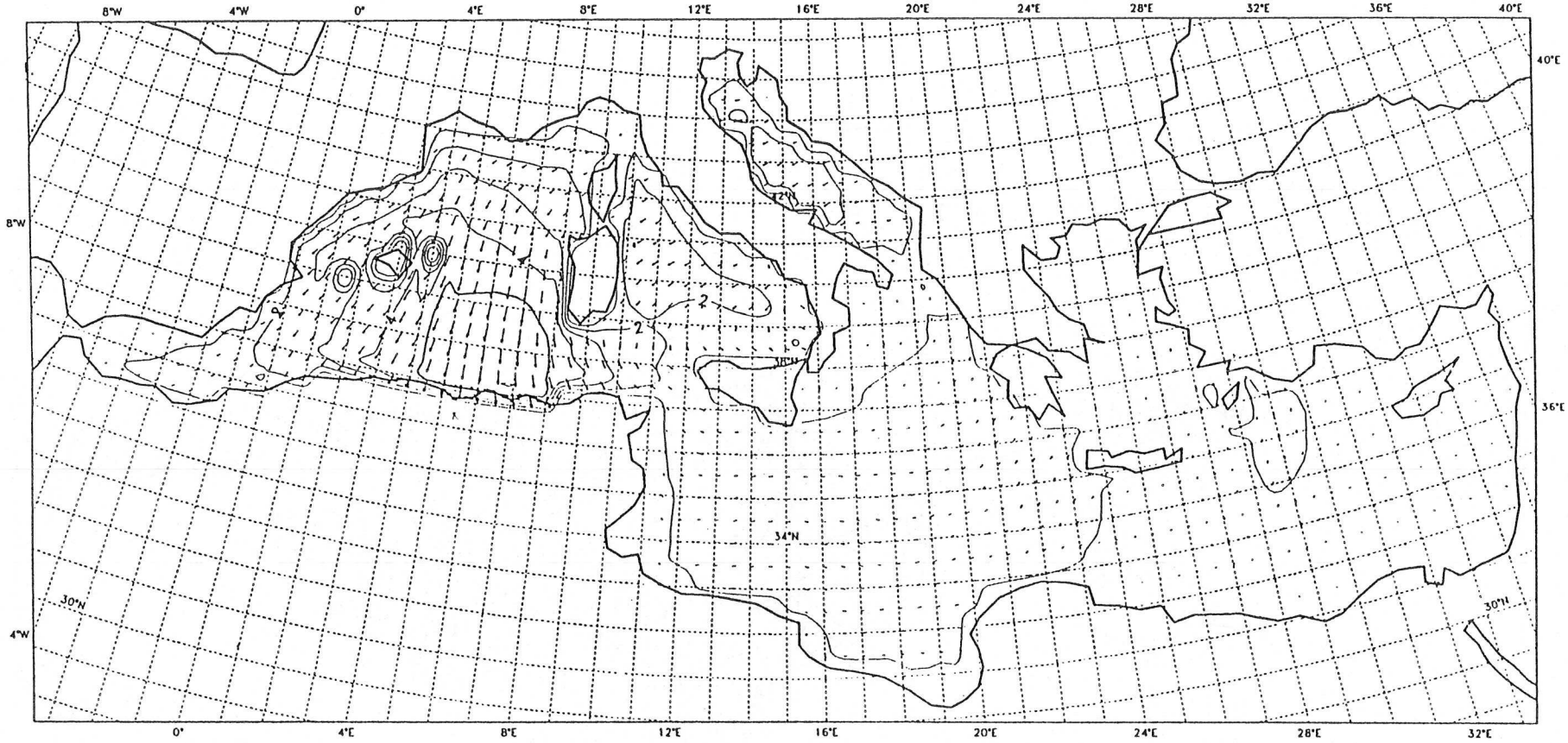

14a

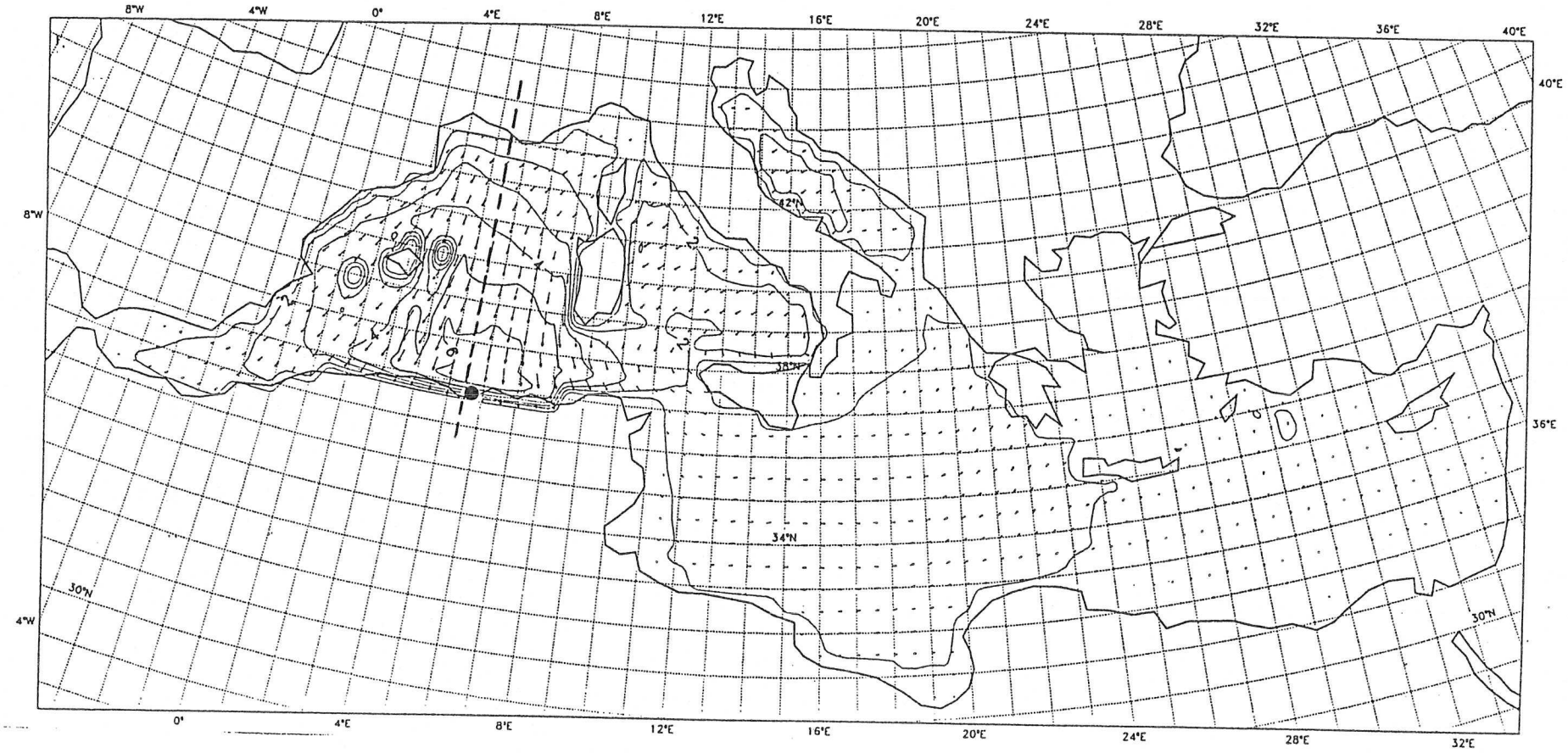
8°W
4°W
0°
4°E
8°E
12°E
16°E
20°E
24°E
28°E
32°E
36°E
40°E
42°N
38°N
34°N
30°N

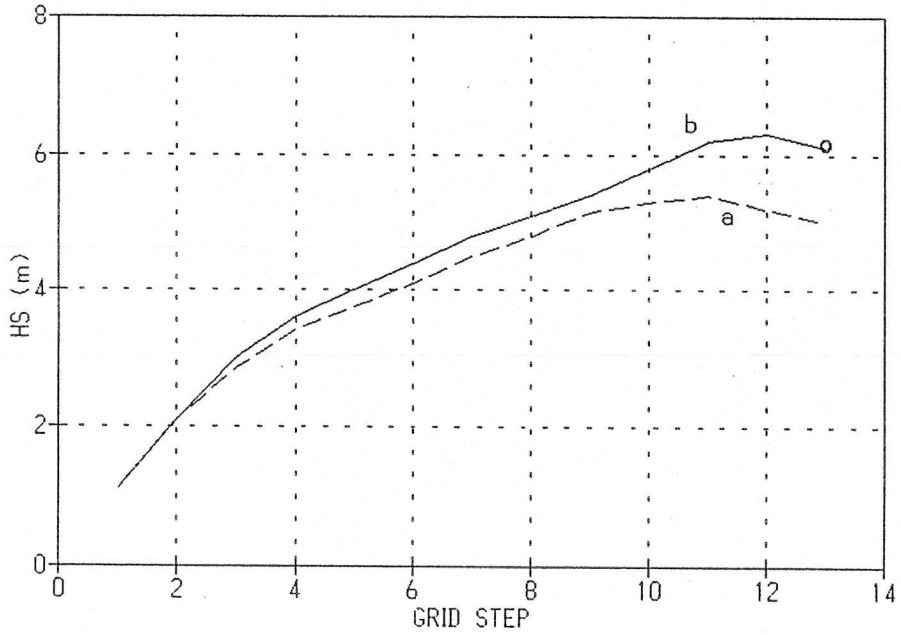
8
6
4
2
0
HS (m)
b
a
0
2
4
6
8
10
12
14
GRID STEP

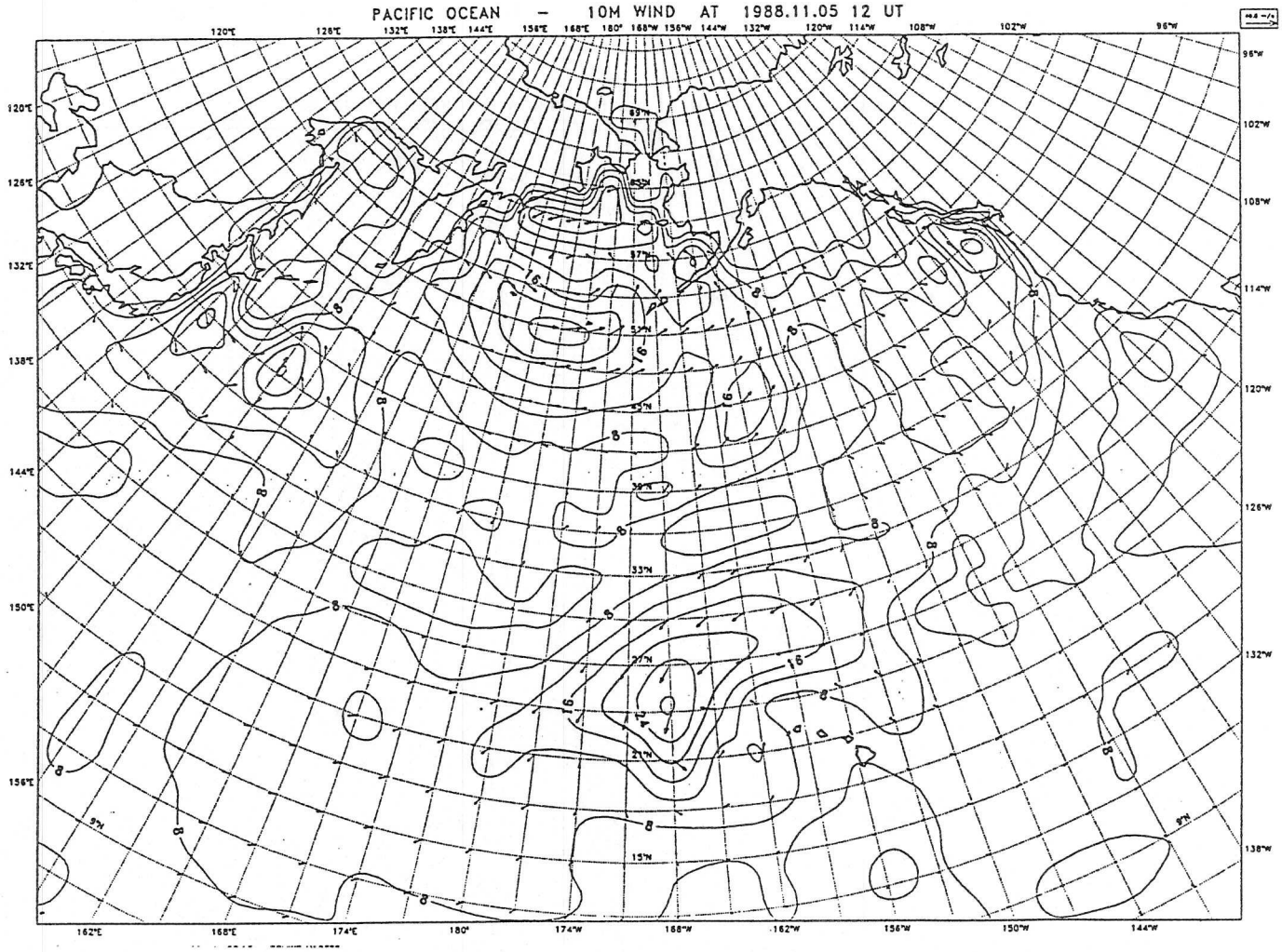
PACIFIC OCEAN - 10M WIND AT 1988.11.05 12 UT
m/s
120°E
126°E
132°E
138°E
144°E
150°E
156°E
162°E
168°E
174°E
180°
174°W
168°W
162°W
156°W
150°W
144°W
138°W
132°W
126°W
120°W
114°W
108°W
102°W
96°W
69°N
63°N
57°N
51°N
45°N
39°N
33°N
27°N
21°N
15°N
9°N
8
16
24

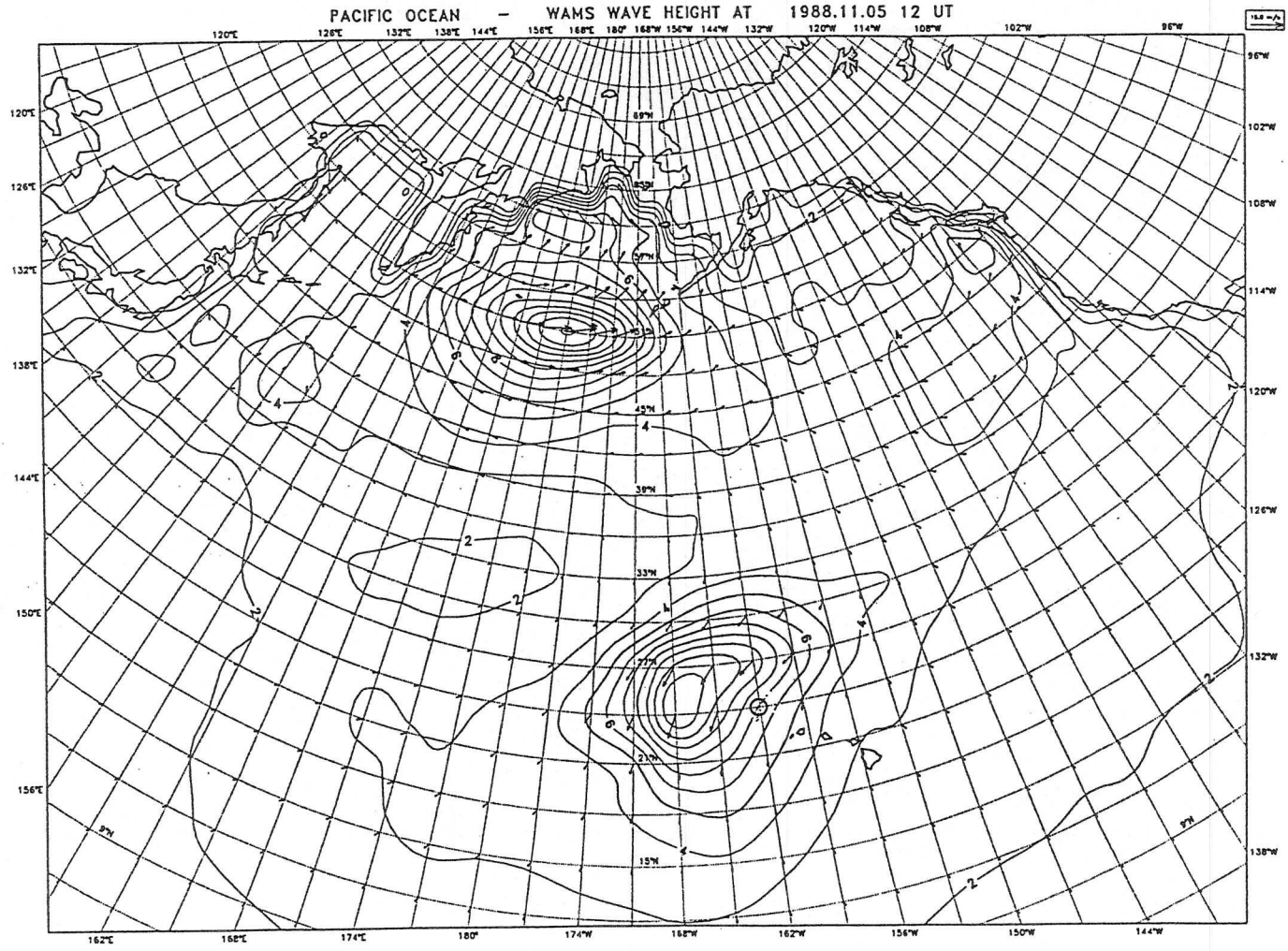
PACIFIC OCEAN – WAMS WAVE HEIGHT AT 1988.11.05 12 UT
120°E
126°E
132°E
138°E
144°E
150°E
156°E
162°E
168°E
174°E
180°
174°W
168°W
162°W
156°W
150°W
144°W
138°W
132°W
126°W
120°W
114°W
108°W
102°W
96°W
69°N
57°N
45°N
39°N
33°N
27°N
21°N
15°N
9°N

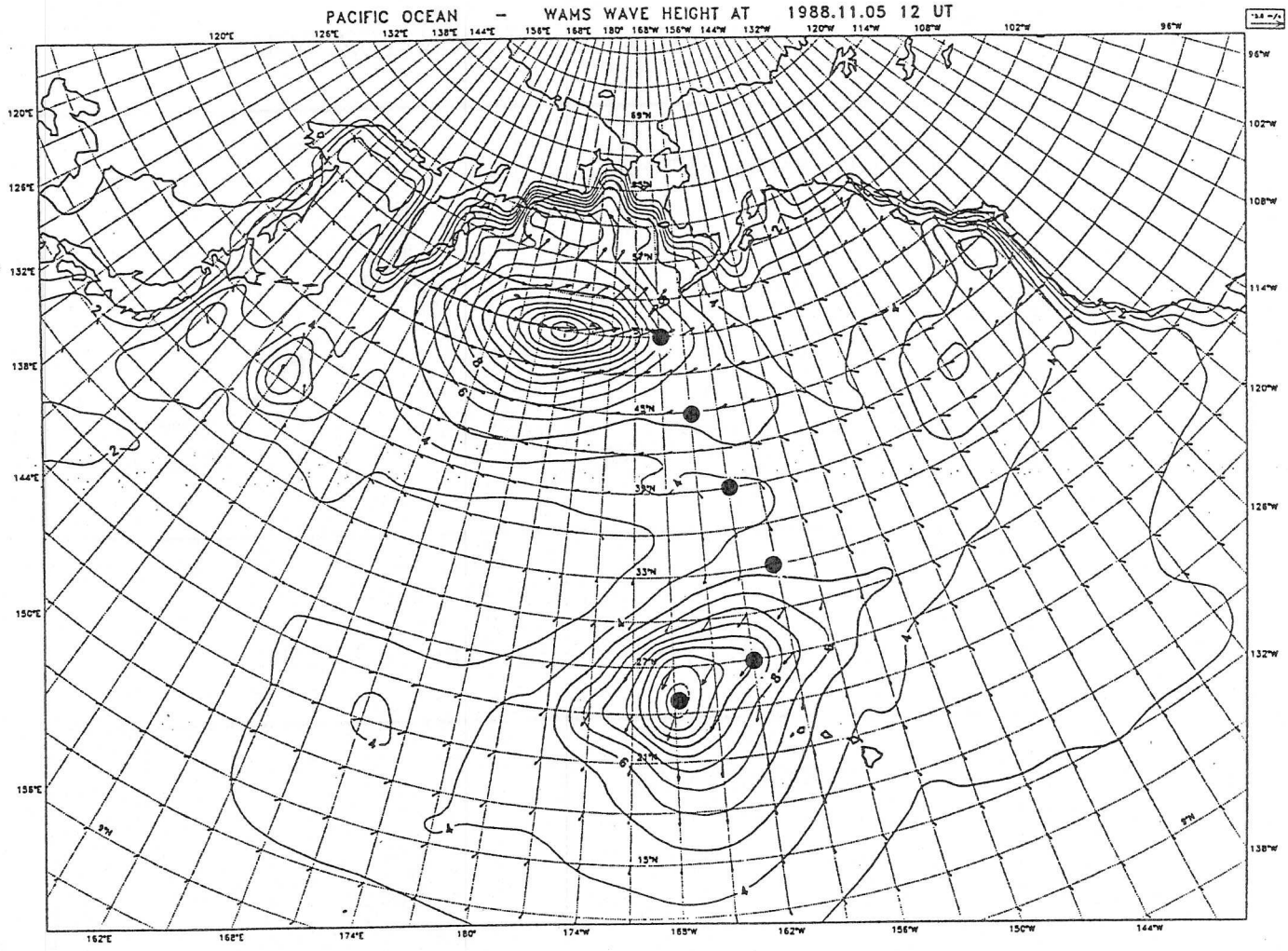
PACIFIC OCEAN – WAMS WAVE HEIGHT AT 1988.11.05 12 UT
120°E
126°E
132°E
138°E
144°E
150°E
156°E
162°E
168°E
174°E
180°
174°W
168°W
162°W
156°W
150°W
144°W
138°W
132°W
126°W
120°W
114°W
108°W
102°W
96°W
69°N
57°N
45°N
39°N
33°N
27°N
21°N
15°N
9°N

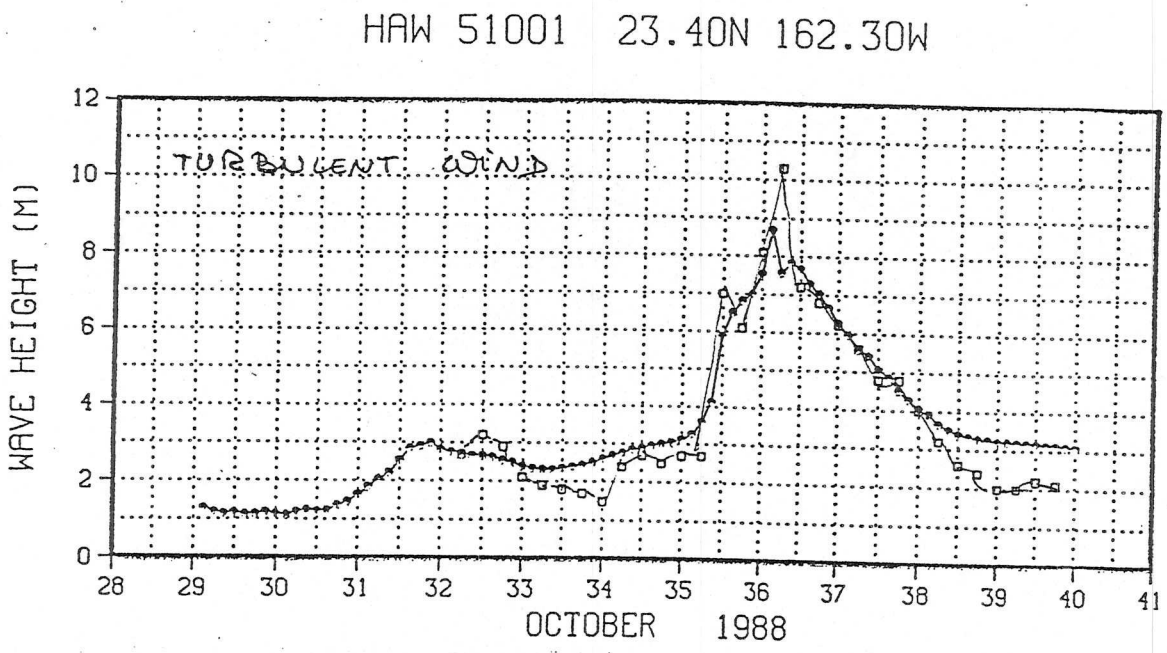
HAW 51001 23.40N 162.30W
TURBULENT WIND
WAVE HEIGHT (M)
0
2
4
6
8
10
12
28
29
30
31
32
33
34
35
36
37
38
39
40
41
OCTOBER 1988

b)

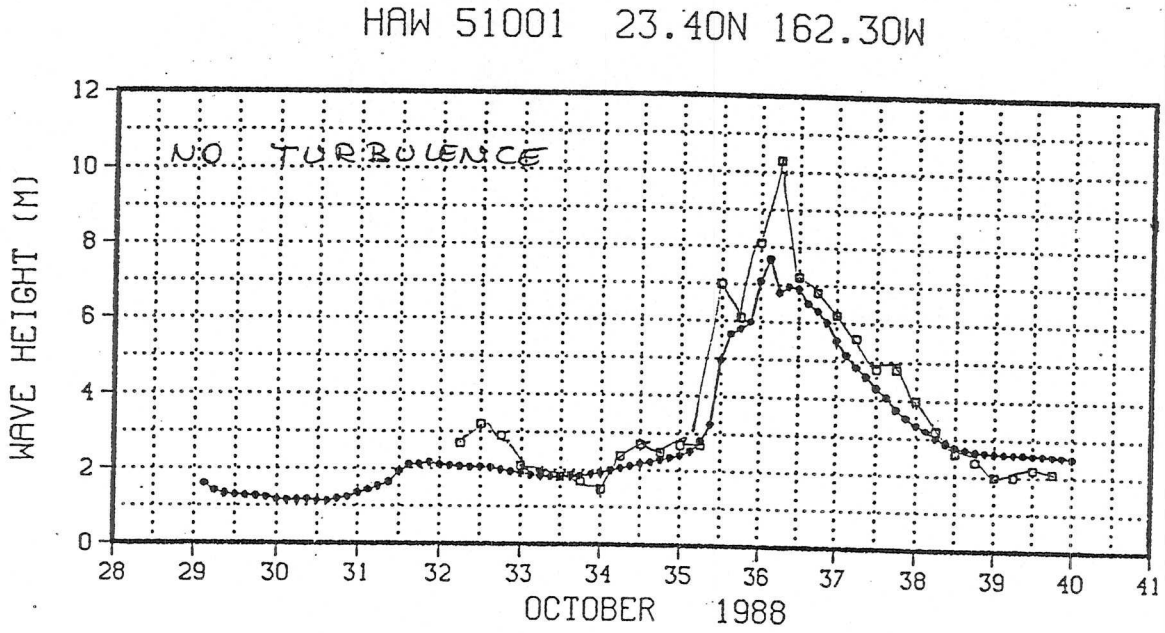
HAW 51001 23.40N 162.30W
NO TURBULENCE
WAVE HEIGHT (M)
0
2
4
6
8
10
12
28
29
30
31
32
33
34
35
36
37
38
39
40
41
OCTOBER 1988

a)

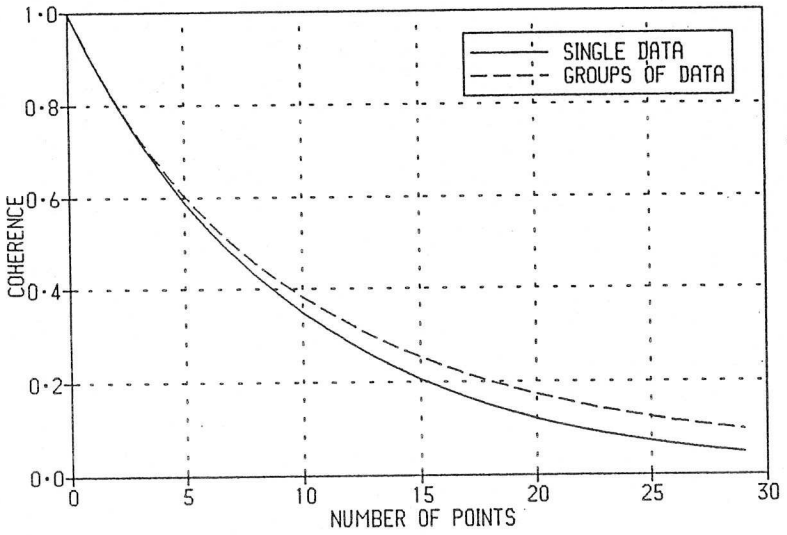
1·0
0·8
0·6
0·4
0·2
0·0
COHERENCE
0
5
10
15
20
25
30
NUMBER OF POINTS
SINGLE DATA
GROUPS OF DATA

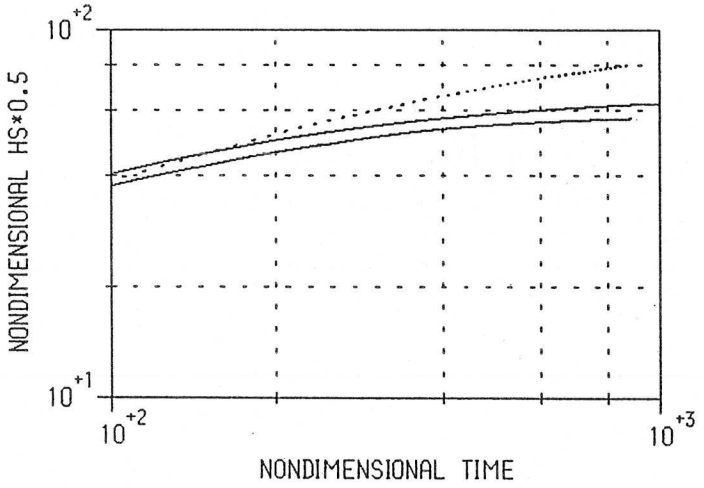
10^{+2}
10^{+1}
NONDIMENSIONAL HS*0.5
10^{+2}
10^{+3}
NONDIMENSIONAL TIME